



Contents lists available at ScienceDirect

Arabian Journal of Chemistry

journal homepage: [www.sciencedirect.com](http://www.sciencedirect.com)

Original article

# Modified locally derived graphene nanoplatelets for enhanced rheological, filtration and lubricity characteristics of water-based drilling fluids



Muftahu N. Yahya<sup>a,b,d</sup>, M.N.A.M Norddin<sup>a,c,d,\*</sup>, Issham Ismail<sup>a,c,\*</sup>, A.A.A. Rasol<sup>a</sup>, Abdul R. Risal<sup>a</sup>, Jeffrey O. Oseh<sup>a,c,d,e</sup>, Faruk Yakasai<sup>a,b</sup>, Eugene N. Nguangna<sup>a</sup>, Sajid Khan<sup>a</sup>, Muhanad Al-Ani<sup>a</sup>

<sup>a</sup> Department of Petroleum Engineering, School of Chemical and Energy Engineering, Faculty of Engineering, Universiti Teknologi Malaysia, 81310, Johor Bahru, Malaysia

<sup>b</sup> Department of Chemical and Petroleum Engineering, Faculty of Engineering, Bayero University, Kano PMB 3011, Nigeria

<sup>c</sup> Malaysia Petroleum Resources Corporation Institute for Oil and Gas (MPRC-UTM), Universiti Teknologi Malaysia, 81310, Johor Bahru, Malaysia

<sup>d</sup> Advanced Membrane Technology Research Centre (AMTEC), Nanostructured Materials Research Group (NMRG) – MD - Frontier Materials, Universiti Teknologi Malaysia, 81310, Johor Bahru, Malaysia

<sup>e</sup> Department of Petroleum Engineering, School of Energy and Energy Engineering, Federal University of Technology, Owerri P.M.B. 1526, Imo State, Nigeria

## ARTICLE INFO

## Article history:

Received 20 June 2023

Accepted 21 September 2023

Available online 27 September 2023

## Keywords:

Graphene Nanoplatelets

Modification

Water-Based Mud

Rheology

Filtration

Triton-X100

## ABSTRACT

Drilling fluid rheology, filtration, and lubricity are fundamental parameters that influence the efficiency and ease of drilling operations. The drilling industry is constantly exploring different research areas for stabilizing and improving these parameters at high temperatures. The use of drilling fluid additives, especially synthetic polymers, poses a threat to the environment. Herein, rice husk char (RHC) was used to synthesize graphene Nanoplatelets (GNP) whose surface is modified with triton-X100 nonionic surfactant. Field emission scanning electron microscopy (FESEM), Fourier transform infrared (FTIR), Particle size distribution (PSD), Energy Dispersive X-Ray Analysis (EDX), and Zeta potential analysis are performed on the synthesized nanomaterials to verify their morphology, functional groups, particle size, elemental composition, and material stability. Synthesized GNP from RHC (GNP-RHC) along with surface-modified GNP-RHC (GNP-TXT) were examined critically and their properties compared using a water-based mud (WBM) formulation. The rheological and lubricity characteristics of all the mud samples were determined before and after hot rolling (AHR), and the filtration properties were determined under API and high pressure high temperature (HPHT) conditions. The TGA results indicate that GNP-TXT nanomaterial resists thermal degradation with 10% weight loss at 300 °C, while the zeta potential analysis indicates the materials are stable. Since the GNP-TXT particles are so well dispersed, the GNP-TXT-based muds worked better than the GNP-RHC-based muds and was more stable at controlling filtration and improving rheological properties. For example, at 1.5 g AHR, the plastic viscosity of GNP-TXT-based mud decreased by 22.2% from 9 to 7 cP, while that of GNP-RHC-based mud decreased from 17 to 7 cP by 59%. Also, the API and HPHT FL of WBM of 11 and 24.8 mL, respectively, were reduced by GNP-TXT-based muds to the range of 8.6 and 9.8 mL for API and 18.6 and 22.3 mL for HPHT. However, GNP-RHC-based drilling muds showed a lower fluid loss control of the WBM between 9.6 and 10.2 mL for API and between 19.6 and 23.6 mL for HPHT. Furthermore, the coefficient of friction of the WBM of 0.45 was decreased with GNP-RHC concentrations between 0.47 and 0.32, while GNP-TXT demonstrated a higher decrease between 0.26 and 0.20.

© 2023 The Author(s). Published by Elsevier B.V. on behalf of King Saud University. This is an open access article under the CC BY license (<http://creativecommons.org/licenses/by/4.0/>).

\* Corresponding authors.

E-mail addresses: [anam@utm.my](mailto:anam@utm.my) (M.N.A.M Norddin), [issham@utm.my](mailto:issham@utm.my)

(I. Ismail).

Peer review under responsibility of King Saud University.



## 1. Introduction

Petroleum exploration has now moved away from shallow oil and gas deposits to deep and unconventional regions due to the decline of shallow fossil fuel resources and growing energy demands (Bayat et al., 2021). The need for high-performance drilling fluid in these harsh environments is therefore critical

<https://doi.org/10.1016/j.arabjc.2023.105305>

1878-5352/© 2023 The Author(s). Published by Elsevier B.V. on behalf of King Saud University. This is an open access article under the CC BY license (<http://creativecommons.org/licenses/by/4.0/>).

## Nomenclature

AHR	After Hot Rolling	MWCNT	Multi-walled Carbon Nanotubes
API	American Petroleum Institute	NP	Nano Particles
BHR	Before Hot Rolling	NS	Nano Silica
CoF	Coefficient of Friction	OBM	Oil Based Muds
CTAB	Cetyl Triammonium Bromide	°C	Degree Celsius
CVD	Chemical Vapor Deposition	pH	Hydrogen Potential
EDX	Energy Dispersive X-Ray	PSD	Particle Size Distribution
FESEM	Field emission scanning electron microscopy	PV	Plastic Viscosity
FL	Fluid Loss	RH	Rice Husk
FTIR	Fourier Transform Infrared Spectroscopy	RHC	Rice Husk Char
Fe <sub>2</sub> O <sub>3</sub>	Ferrous Oxide (Iron Oxide)	ROP	Rate of Penetration
GNP	Graphene Nanoplatelets	SDBS	Sodium Dodecyl benzene sulfate
GNP-RHC	Graphene Nanoplatelets from rice husk char	SDS	Sodium Dodecyl-sulfate
GNP-TXT	Graphene Nanoplatelets with triton-X100	TEM	Transmission Electron Microscopy
GS	Gel Strength	TGA	Thermogravimetric Analysis
HPHT	High Pressure and High Temperature	Triton X-100	4-(1,1,3,3-tetramethylbutyl) phenyl-polyethylene glycol
KOH	Potassium Hydroxide	WBM	Water Based Muds
KCl	Potassium Chloride	YP	Yield Point
LPE	Liquid-phase Exfoliation		
MGNF	Multilayered Graphene Nano flakes		

(Medhi et al., 2021). Oil-based muds (OBMs) and water-based muds (WBMs) are the two most important types of drilling muds, with WBMs being more feasible and appealing for drilling than OBMs due to environmental concerns and cost considerations (Salih et al., 2016). WBMs are extensively used because of their low cost and ease of preparation (Rafieefar et al., 2021). Drilling fluids are primarily used to control formation pressure and remove surface cuttings from the wellbore during drilling operations (Heshamudin et al., 2019; Majid et al., 2019). It is also important to sustain an efficient drilling process and reservoir stability by maintaining drilling mud rheological properties, such as density, plastic viscosity (PV), apparent viscosity (AV), yield point (YP), gel strength (GS), filtrate loss volume, and lubricity (Aftab et al., 2017; Salahudeen et al., 2020). The carrying capacity of WBM is directly related to its rheological properties. WBMs that have a higher viscosity and yield stress generally have a better conveying ability (Heshamudin et al., 2019). Wellbore stability is strongly influenced by the filtration characteristics of WBMs. As wellbore stability is compromised by water infiltration into porous formations, complications such as stuck piping and formation collapse may result (Sensoy et al., 2009; Tian et al., 2022).

Nanotechnology has become widely used in every aspect of technology and engineering over the last two decades. It has been shown that nanoparticles (NP) can solve many complex drilling problems, including wellbore instability, pipe sticking, loss of circulation, torque, and drag (Amanullah and Al-Tahini, 2009). Drilling fluids can be improved by adding NPs to reduce filtrate loss, reduce friction coefficients, and improve shale stability (Oseh et al., 2020; Perumalsamy et al., 2021). The shape, size, concentration, and surface charges of NPs in drilling fluid are mainly responsible for the performance of NPs in drilling fluid (Salih and Bilgesu, 2017). It is possible to reduce the amount of solid contents in drilling fluids significantly with the addition of NPs. Mud systems with high solid content may have a decrease in the rate of penetration due to increased viscosity (Irawan et al., 2018). The unique properties of graphene have made it one of the most promising nanomaterials. In addition to being a great conductor of electricity and heat, it is optically transparent yet impermeable to gases because it is so dense. This material has advantages in both physical and electrical properties. For instance, it is strong, has a high Young's modulus, has good thermal conductivity, and has a high electron

mobility (James and Tour, 2013). Graphene, however, has a distinct advantage over other carbon-based materials, such as fullerenes or carbon nanotubes (CNTs). In contrast to CNTs, which are grown by the catalytic action of nanoparticles in the presence of carbon-containing gases. No metallic impurities can be found in graphene and its derivatives (Szunerits and Boukherroub, 2016). The technology can be applied to a variety of applications, such as drilling (Ahmad et al., 2021), cementing (Massion et al., 2022; Sun et al., 2017), enhanced oil recovery (Hamdi et al., 2022; Ilyas et al., 2020), desalination (Gontarek-Castro et al., 2021), oil spill cleanup (Sultanov et al., 2020; Tao et al., 2019), and stabilizing emulsions (Sie Yon et al., 2013). GNPs have been used as a drilling fluid additive in several laboratory experiments (Arain et al., 2022; Ridha et al., 2018; Tofighy and Mohammadi, 2019), as well as oil well cement additives (Alkhamis and Imqam, 2018; Tabatabaei et al., 2022) and in the field (Taha and Lee, 2015). According to Aftab et al. (2017), the PV and GNP concentration increased linearly with reduced filtrate loss.

The four main methods used to synthesize graphene include chemical vapour deposition (CVD), graphite exfoliation, epitaxial growth on silicon carbide, and graphene oxide chemical reduction. In addition to its essential benefits over other techniques, chemical activation has been extensively studied by researchers as both the previous methods entail high temperatures, high vacuums, and expensive experimental setups (Hussain et al., 2020; Muramatsu et al., 2014; A. Raghavan et al., 2020). Since chemical activation has a lower activation temperature, well-defined micro pore size distribution, higher yields, and ultrahigh surface area, as well as well-ordered structure and surface functionalities, it is particularly preferred for converting biomass and other waste materials into graphene nanosheets, activated carbon, graphene oxide, and porous graphene (Linares-Solano et al. 2014, Wang et al., 2011). In contrast to other chemicals, potassium hydroxide (KOH) is preferred because it is completely reactive with carbon precursors and converts metallic oxides into soluble carbonates (Jiang et al., 2018; Muramatsu et al., 2014; Z. Wang et al., 2016). It is shown that chemical activation processes are more economical, more scalable, and more reliable (Che Othman et al., 2020; N. Raghavan et al., 2017; Sudhan et al., 2017). Using KOH and activated carbon as protective barriers against oxidation, (Muramatsu et al., 2014) reported the first synthesis of graphene

from rice husk (RH). A number of technologies are needed to make use of RH effectively, as it is one of the most widely produced agricultural materials in the world (Tuck et al., 2012). As part of green production, toxic chemicals, and natural precursors are used less frequently (Singh et al., 2017). In recent years, researchers have established a green method for producing graphene using eco-friendly biomass resources (e.g., foodstuffs, sugar, alfalfa plants, and chitosan) (Muramatsu et al., 2014; Ruiz-Hitzky et al., 2011; Singh et al., 2017; Y. Zhu et al., 2010). An activated GNP was produced from carbonized brown RH by heating it with KOH. With this approach, super-thin crumpled silk-veil-wave nanosheets are produced with a high surface area of 1225 m<sup>2</sup>/g and a high porosity (Sankar et al., 2017).

In spite of graphene's many advantageous properties, distinct graphene NPs may adhere to each other by forming a bond-like graphite. It is possible that graphene will be bundled up and summed up by this interaction, making it difficult to disperse in aqueous solutions (Kumar and Guo, 2011). Due to the unique properties associated with graphene sheets, avoiding aggregation was of particular importance to keep them separate. It is reported that steric or electrostatic repulsion can achieve this purpose (Hong and Kim, 2012). The chemical modification of graphene can result in unprecedented changes to the properties of the material (Guardia et al., 2011; Wajid et al., 2012). Noncovalent methods of dispersing carbon nanomaterials have extensively employed surface-active agents, more commonly known as surfactants. It is known that surfactants have two components, a polar hydrophilic head, and a hydrophobic tail, which is usually made up of a hydrocarbon chain (Morrison and Ross, 2002). Graphene Nanoplatelets were functionalized noncovalent with Triton X-100 and DTAB surfactants to influence their dispersions in aqueous drilling fluids (Ibrahim et al., 2019). As a result, triton X-100 exhibits the highest dispersion rate against DTAB, and is also less shear stress sensitive than DTAB at an equal share rate, an important characteristic for drilling fluids. Graphene-modified samples were found to be more fluid-stable than conventional clay-based samples and to have less filter loss (Kosynkin et al., 2012). Further, Aftab et al. (2017) proved that graphene-modified fluids showed substantial improvements in rheology, significantly decreased filter loss volume, and showed improvements in shale inhibition.

A number of polymer-based additives have been investigated for their use as rheological enhancers and FL control agents (Hamad et al., 2020; Hasan et al., 2018). The rheological properties of synthetic polymers have made them widely used as drilling mud additives over the decades (Fink, 2015; Safi et al., 2016). Due to various limitations, such as thermal instability, salt intolerance, cost inefficiency, and environmental aloofness, synthetic polymers are not suitable for use as drilling fluid additives (Tchameni et al., 2019; Q. Zhu et al., 2018). Several environmentalists have expressed concern over their usages, production methods, and discharges (Amanullah and Yu, 2005; Saboori et al., 2018; Xu et al., 2019). Drilling mud additives are having a catastrophic impact on the environment and concerns have increased globally for the protection of the environment (Elkatatny et al., 2016). Consequently, a new generation of thermally stable, environmentally friendly, and cost-effective fluid additives is needed to improve rheological properties with minimal effects on the environment and improve drilling mud performance.

This is the main motivation behind this study. In addition, the degradation of polymers occurs at elevated temperatures, which makes it possible to use non-polymeric additives that function effectively in HPHT conditions. Furthermore, recycling natural materials or waste materials is often emphasized in the oil and gas industry to improve economics and protect the environment. Presently, the main challenge in drilling fluid formulation is

providing environmentally safe, thermally resistant, and cost-effective materials. This study is aimed at synthesizing an environmentally friendly drilling fluid additive with enhanced material physical and thermal characteristics. The influence of the synthesized nanomaterial will be examined in a laboratory setting for rheological, filtration, and lubricity characteristics in WBM. In recent years, numerous studies have been conducted on the impact of GNPs on drilling fluid performance, stability, and dispersion, most involving commercially sourced GNPs incorporated into aqueous formulations. It is for the first time that a study will be conducted to examine the usability of a modified bio-derived GNPs in WBM formulation. Through a comprehensive investigation, modified RH-derived nanomaterial was examined at high and ambient temperatures for its impact on WBM.

As drilling fluid formulations become more sophisticated, renewable materials have become more popular as additives. A number of research articles on drilling fluids (Gautam et al., 2021), nano additives (Oseh et al., 2023), and graphene nanoplatelets (Aramendiz and Imqam, 2019) have been published in the literature. The main focus of these articles is on drilling fluid rheological behaviour, filtering properties, lubricity, among other applications. There have been a number of studies reported in the past that used commercial GNP (Husin et al., 2018). As a result of their superior thermal properties, mechanical properties, high aspect ratios, and plate-like shapes, GNPs are considered the next generation of nanomaterials for the oil and gas industries (Tofighy and Mohammadi, 2019). A recent paper evaluating the effectiveness of GNPs as a filtration material for WBM was published by (Ridha et al., 2018). According to the study, GNPs performed much better than silica nanoparticles for filtration at high temperatures. Arain et al. (2022) studied the performance of a novel drilling fluid enhanced with GNPs under high temperatures. There was a 11% and a 42% improvement in PV and YP associated with GNPs in the said study. A very low-cost drilling fluid formulation was one of the motivations for investigating raw biomass for the production of GNP. A further problem is the high cost of commercial GNP per few grams, which has a negative impact on drilling operations due to its high price tag. We believe that this is the first study to use rice husk-derived GNP as a component in WBM. Our research aims to provide insight into the use of agricultural waste material in improving drilling fluid rheological properties, filtration properties, and lubricity properties. Hence, the purpose of this work is to exploit the research gap by repurposing agricultural waste to make GNP and investigating the effects of this compared to water-based bentonite suspensions in drilling fluids.

The objective of this study is to examine the performance of triton X-100-modified derived GNPs at ambient and reservoir temperatures with respect to WBMs. Compared to traditional nanomaterials, modified nanomaterials demonstrated enhanced performance and characteristics. In order to analyse the properties of the synthesized nanomaterials, morphology, thermal stability, material size, and elemental compositions/purities are measured. According to the recommended standard procedures for testing the characteristics of water-based drilling fluids by American Petroleum Institute (API RP 13B-1, 2009), the rheological behaviour, filtration characteristics, and fluid lubricity are investigated at ambient and reservoir temperatures.

As a follow-up to section 1 (Introduction), the rest of the study is organized as follows: Section 2 (Materials and methods) covers the description of the materials, synthesis methods, characterizations, and sample testing. The results and discussions of the study are presented in Section 3 (results and discussions). As for Section 4 (Summary and conclusions), it summarizes the study results, findings, and mechanisms and draws a conclusion.

## 2. Materials and methods

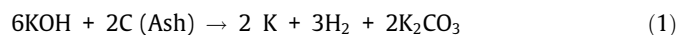
### 2.1. Materials

RH were obtained from Kilang Beras Jelapang Selatan Sdn. Bhd., a local paddy mill in the state of Johor Malaysia. KOH, triton-X100, and potassium chloride (KCl) were purchased from Quality Reagent Chemical Product (QReC), sodium hydroxide (NaOH), and polyanionic cellulose (PAC) were purchased from R&M chemicals. Barite and Bentonite were provided by Scomi oil tools. All materials were used as received without further modification and purification.

### 2.2. Synthesis of RH-derived graphene

RH-derived graphene was prepared using a chemical activation method with several modifications (Fig. 1) (Muramatsu et al., 2014). The procedure was performed under an air tight atmospheric conditions using KOH as an activating agent (Arifin et al., 2021). In this study, the black sample that was extracted from calcinated RH was termed rice husk char (RHC). Raw RH was initially washed with tap water and dried in an oven at a temperature of 600 °C for 24 h. Ten grams of the raw RH was thermally treated at a pre-treatment temperature of 600 °C in a furnace at a heating rate of 10 °C/min for 2 h to obtain RHC. The yield of RHC from raw RH is 42% (approx.). The activated RHC was mixed with KOH in a 1:5 proportion, and the corresponding amount of RHC was mixed with the ratio of KOH pellets in distilled water. The solution was filtered and dried in an oven at 80 °C for 24 h. The dried RHC/KOH powder was put into a double crucible setting as shown in Fig. 1. To prevent oxidation at high temperatures, activated carbon was used. The crucible setting was lastly placed into a furnace for 2 h at 900 °C, and graphene powder was finally obtained. A similar mechanism has been proposed (Zhu et al., 2007) for the activation of carbon for graphene synthesis. Carbon is first activated through its reaction with KOH (Eq. (1)), followed by the decomposition of  $K_2CO_3$ , or by the reaction of  $K/K_2CO_3/CO_2$ . Activation can be sum-

marized using the following chemical equations (Sankar et al., 2017).



### 2.3. Surface modification of RH-derived graphene

A method of surface modification was used to modify GNP-RHC according to (Qamar et al., 2019; Yasin et al., 2013). In the first step, about 20 g of the synthesized GNP-RHC powder was sonicated in 150 mL of water for 30 min. Following the dispersion of GNPs, 100 mL of water was treated with the desired amount of surfactant (TritonX-100), followed by stirring at room temperature. After transferring the mixture to a stirrer plate at 60 °C, it was stirred for 2 h. Following that, the solution was kept unattended for one week. Finally, Whatman cellulose acetate membranes 0.45 μm, 25 mm 100/pk was used to filter the products and dry them in a laboratory oven for 72 h at 60 °C. As a result, the functionalized graphene sample GNP-TXT was produced.

### 2.4. Characterizations

Master Sizer 3000 Laser Particle Size Analyser (LPSA) (Malvern Instruments, Worcestershire, Britain) was used to measure the mean particle size and PSD. With the Perkin-Elmer Spectrum Two (FTIR instruments, Houston, USA) the study measured the FTIR from 1000 to 4500  $cm^{-1}$ , which allowed to identify the functional groups. FESEM and EDX were used to study structure, morphology and elemental characteristics. Using an Air Lock chamber after platinum coating for higher magnifications, Carl Zeiss (Germany) Supra 55 model was used, and Hitachi JEM-2100UH, Japan, was used for high-resolution TEM. A Netzsch-STA 449 Jupiter instrument (TA instruments, Germany) was used for measuring

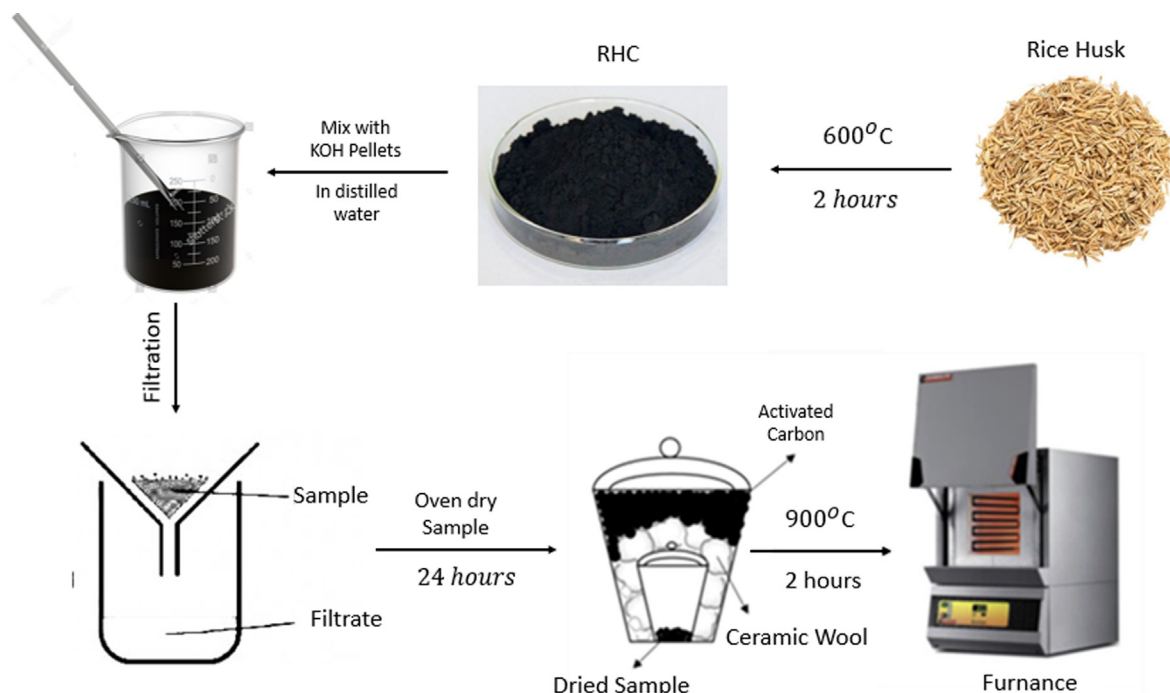


Fig. 1. Methodology Flow chat for GNP-RHC.

the thermal properties. In a protective nitrogen gas environment, about 0.02 g of the material samples were sealed in aluminium pans and scanned from 30 °C to 850 °C for 10 °C a minute, to determine the weight loss of the samples.

To investigate their stability under varying pH conditions, the zeta potential of GNP-RHC and GNP-TXT particles in aqueous dispersion was measured. Deionized water was added to Na-MMT to obtain a concentration of 0.5 g/l. Nano additives with varying pH values were incorporated into the dispersion. In a room-temperature Malvern instrument at Zetasizer3000 electric potential and granularity meter, the zeta potential of the particles was measured after vigorous stirring for 24 h.

## 2.5. Drilling fluids preparations

In this study, GNP-RHC and GNP-TXT nano powders were examined for their ability to improve WBM rheological characteristics and filtration ability. Different drilling fluid formulations were tested by varying the concentration of additives. The preparation of drilling fluid was conducted according to API RP 131 (API, 2009). A Hamilton Beach mixer was used to mix the additives at a high shear rate (21,000 rpm). In 350 mL of tap water, 15 g of bentonite were dissolved for 15 min, and then 0.45 g of soda ash ( $\text{Na}_2\text{CO}_3$ ) was added for five minutes. The following materials were mixed for 5 min sequentially: 1.5 g of PAC-UL and 3.4 g of KCl. The base mud was then obtained by adding Barite (25 g) and mixing it for 15 min. GNP-RHC and GNP-TXT materials additives were applied at various concentrations, as shown in Table 1. The fluid samples were formulated in multiples of 350 mL to carry out all the required tests from rheological, filtration and lubricity properties before and after hot rolling.

## 2.6. Measurement of rheological properties

A fluid's rheology is determined by its resistance to flow. Every drilling fluid must have this feature and should be designed correctly (Gamal et al., 2019; Salahudeen et al., 2020). Density measurements of WBM were conducted using mud balance. After the lid of the balance cup had been removed, a sample of drilling fluid was placed inside. To ensure that the cup was fully filled with drilling fluid, some drilling fluid was allowed to overflow from a hole in the lid. Lastly, the knife-edge was placed in the fulcrum of the arm balance. Until the vial was centred, the rider was moved along the graduated arm. The density value was then measured accordingly.

Viscometers (Fann, Houston, TX, USA) were used to determine the rheological properties of WBM. To test the integrity of the equipment, the viscosity of distilled water was tested after the equipment was switched on and stabilized. The mud sample was poured into the viscometer cup and placed it on the stand. When the rotor sleeve was immersed exactly up to the fill line, the stand was adjusted and held in place. The dial readings at 600 rpm to 3 rpm were carefully recorded for each drilling fluid formulation.

Based on the dial readings obtained, the PV, YP, and AV of the mud samples were calculated using eqs. (4) to (6).

$$PV = \theta_{600} - \theta_{300} \quad (4)$$

$$YP = \theta_{300} - PV \quad (5)$$

$$AV = \theta_{600}/2 \quad (6)$$

where PV (cp), YP (lb/100ft<sup>2</sup>) and AV (lb/100ft<sup>2</sup>).

A drilling fluid's GS reflects the fluid's thixotropic properties and is usually reported as a 10 sec GS and 10 min GS based on the maximum dial reading at 3 rpm after its been at rest for 10 s and 10 min. All the mud properties (PV, YP, GS10 sec, and GS10 min) were measured before hot rolling (BHR) at 78°F and after hot rolling (AHR) at 250°F for 16 hrs.

## 2.7. Measurement of filtration properties

If a drilling mud is designed properly, then its filtration rate should be minimal. High temperatures can cause drilling fluid degradation and excessive filtrate intrusion, which results in a loss of money and resources. It is therefore the responsibility of the drilling engineer to design drilling fluids with the best specifications possible (Cameron, 2001; Pirazad et al., 2018). Testing the filtration of mud is crucial to determining the fluid loss and the thickness of the filter cake. Physical and chemical reactions within the drilling mud, as well as particle quantity, temperature, and pressure, control the parameters in drilling mud. In the current study, both API and HPHT filtration tests were conducted. A Fann Instrument Company API filter press (Houston, TX, USA) was used for API filtration, and a fixed pressure of 100psi was maintained at room temperature for 30 min. An HPHT static filtration test was performed using the Ofite HPHT filter press in order to mimic the static filtration behaviour of drilling mud. HPHT tests were conducted with a constant pressure of 500psi and a temperature of 250 °C. Once the access mud was removed from the filter cake, it was stored properly. In the end, a digital Vernier calliper was used to measure the thickness of the filter cake.

## 2.8. Measurement of mud lubricity

Drilling fluids are tested for lubricity coefficient using an OFITE tester. Deionized water is used to calibrate the equipment prior to testing the mud samples. After calibration, mud samples are placed in the metal cup. In the testing machine, two hardened steel surfaces, a rotating ring, and a stationary block are subjected to a force of 150 in-lb at 60 rpm. A 25 °C and 121 °C lubricity test is performed on each mud sample. After 5 min of observation, data is recorded for each test. Finally, the lubricity coefficient is determined by using eq. (7) and (8).

$$\text{Correction Factor} = \frac{\text{Standard Meter Reading for Deionized Water}}{\text{Meter Reading Obtained in Deionized water Calibration}} \quad (7)$$

**Table 1**  
The composition of WBM with and without nano additives.

	Base Mud	GR1	GR2	GR3	GR4	GT1	GT2	GT3	GT4	Mixing Time (minutes)
Water (mL)	350	350	350	350	350	350	350	350	350	15
Bentonite (g)	15	15	15	15	15	15	15	15	15	5
$\text{Na}_2\text{CO}_3$ (g)	0.45	0.45	0.45	0.45	0.45	0.45	0.45	0.45	0.45	5
PAC UL (g)	1.5	1.5	1.5	1.5	1.5	1.5	1.5	1.5	1.5	5
KCL (g)	3.4	3.4	3.4	3.4	3.4	3.4	3.4	3.4	3.4	5
Barite (g)	25	25	25	25	25	25	25	25	25	15
GNP-RHC (g)	0	0.5	1.0	1.5	2.0	0	0	0	0	15
GNP-TXT (g)	0	0	0	0	0	0.5	1.0	1.5	2.0	15

$$\text{Lubricity Coefficient} = \frac{\text{Meter Reading} \times \text{Correction Factor}}{100 \text{ Pounds}} \quad (8)$$

### 3. Results and discussions

#### 3.1. Characterization of synthesized GNP-RHC and modified GNP-TXT

##### 3.1.1. PSD analysis

With a decrease in particle size, there will be an increase in surface area per unit volume or mass. Surface area indicates more contact area, better cohesion, and better particle grip. Fig. 2 shows the PSD for the GNP-RHC and GNP-TXT. The GNP-RHC in Fig. 2(a) indicated that the size distribution by intensity has two peaks. Recorded as 645.2 nm for peak 1 at 20.5 % with 177.4 nm standard deviation. Peak 2 with a size of 127.6 nm having 79.5 % and a standard deviation of 23.75 nm. The modified GNP (GNP-TXT) in Fig. 2 (b) also has two peaks, with peak 1 having a size of 392.8 nm at 6.6 % with a standard deviation of 92.52 nm. Peak 2 has a particle size of 97.34 nm of 93.4 % at a standard deviation of 18.10 nm. The median particle size (D50) of GNP-TXT is 97.34 nm and the particle size distribution is between 80 and 250 nm. The difference in par-

ticle size between GNP-TXT and unmodified (GNP-RHC) particles is a result of less agglomeration and aggregation.

##### 3.1.2. FTIR

GNP-TXT and GNP-RHC FTIR spectra are shown in Fig. 3. FTIR spectrum analysis of the Triton-treated GNP-RHC with its main infrared peaks and assigned bonds is shown in Table 2. A broad peak at  $3100 \text{ cm}^{-1}$  can be observed in the GNP-RHC FTIR spectrum displayed in Fig. 3 arising from vibrations of O-H and carbonyl (C = O) stretching (Fu et al., 2010; Hu et al., 2010; Uddin et al., 2013). The peak at  $1464 \text{ cm}^{-1}$  is observed as a deformation through (O-H) and the peak at  $1337 \text{ cm}^{-1}$  is a stretching through (C-OH). The peak at  $1132 \text{ cm}^{-1}$  indicates that GNP-RHC sheets contained epoxy groups. Moreover, based on some literature references, some GNPs were found to contain oxygen functional groups (hydroxyls, carboxyls, and epoxy groups) at 1464, 1337, 1239, 1182, and  $1132 \text{ cm}^{-1}$  (Saleem et al., 2018; Valencia et al., 2018). The characteristic peaks of GNP-RHC disappeared or shrunk when modified with Triton X-100. As a result of the carbon skeleton stretching of the benzene ring, GNP-TXT spectra exhibit weak and sharp bands at 1606, 1540, and  $1504 \text{ cm}^{-1}$ . The bands of  $1182 \text{ cm}^{-1}$  and  $1239 \text{ cm}^{-1}$  were formed by stretching C-OH (Qamar et al., 2019). A small peak at around  $3650\text{--}3850 \text{ cm}^{-1}$  in

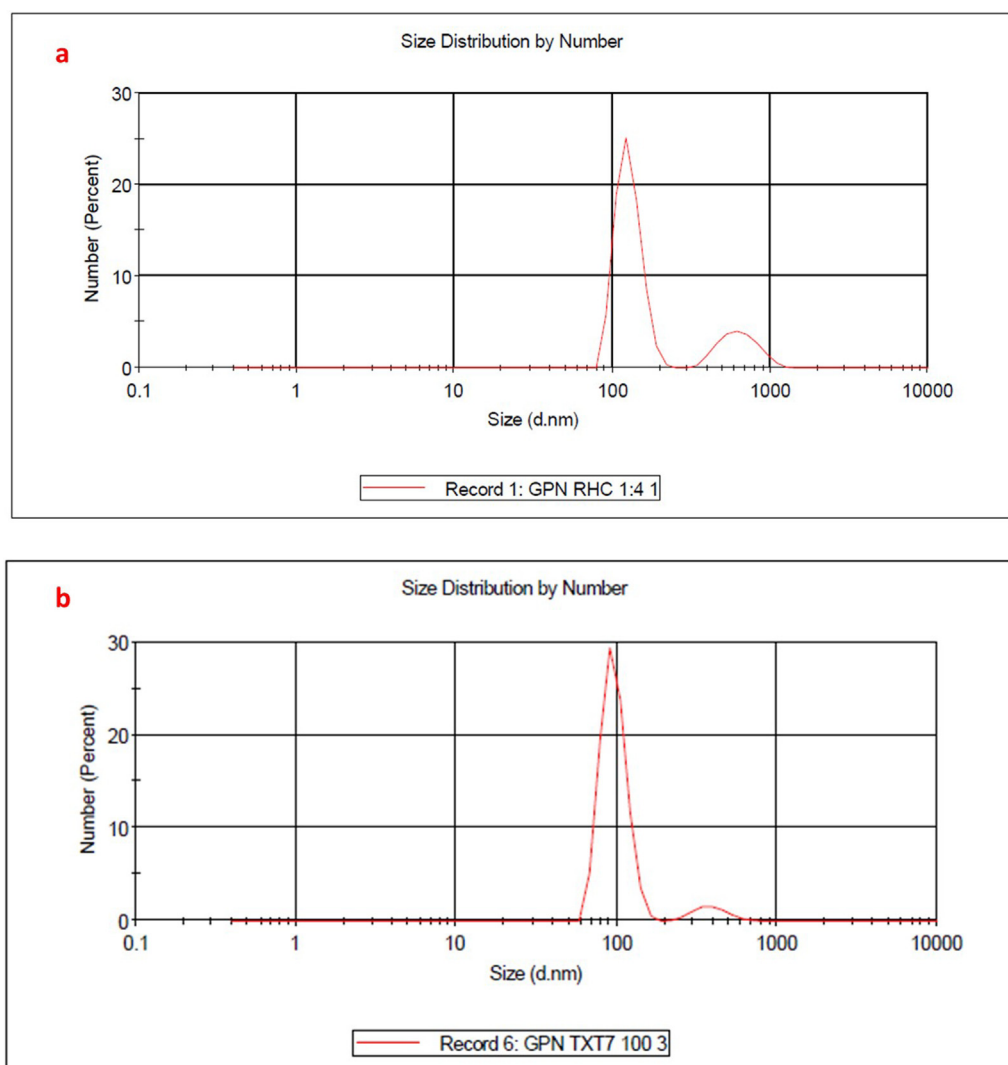


Fig. 2. Particle size distribution for (a) GNP-RHC and (b) GNP-TXT.

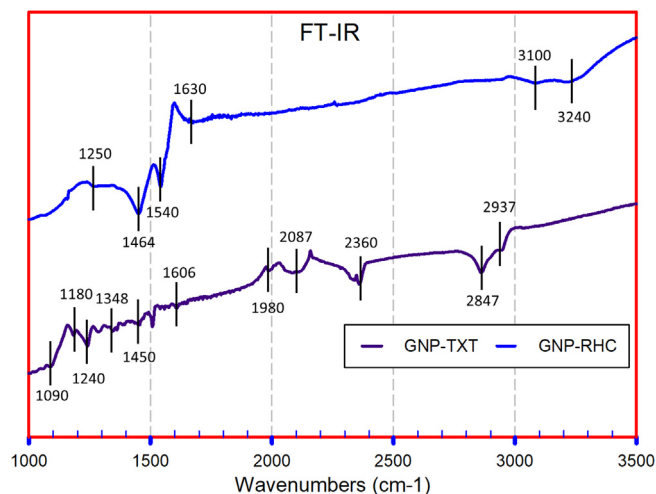


Fig. 3. FT-IR spectra of GNP-RHC, and GNP-TXT.

Table 2

Infrared peaks and functional groups for GNP-TXT.

Peak/cm <sup>-1</sup>	Interpretation
3389	O–H stretching vibration
2917 and 2937	C–H stretching vibration (sp <sup>3</sup> hybridization)
1606, 1540, and 1504	C = C sp <sup>2</sup> carbon skeletal stretching vibration (Benzene ring)
1239 and 1182	C–OH stretching vibration
1240	C–O stretching vibration (carboxylic group)
1056 and 1140	C–O stretching vibration (Ester band)

the GNP-TX spectrum indicates that triton surfactants contain fewer copolymers. In accordance with these observations, it is safe to confirm that surfactant molecules were effectively grafted on the GNP-RHC surfaces (Dong et al., 2008).

### 3.1.3. Thermogravimetric analysis

A thermogravimetric analysis (TGA) was conducted on GNP-RHC and GNP-TXT materials surfaces to determine the percentage of oxygen-containing groups and the thermal degradation of block copolymers. From the GNP-RHC spectrum (Fig. 4), the material lost 36% of its total weight at 850 °C and around 12% by weight at 350 °C. The first loss of weight occurred between 70 and 140 °C which can be attributed to the evaporation of water from the sam-

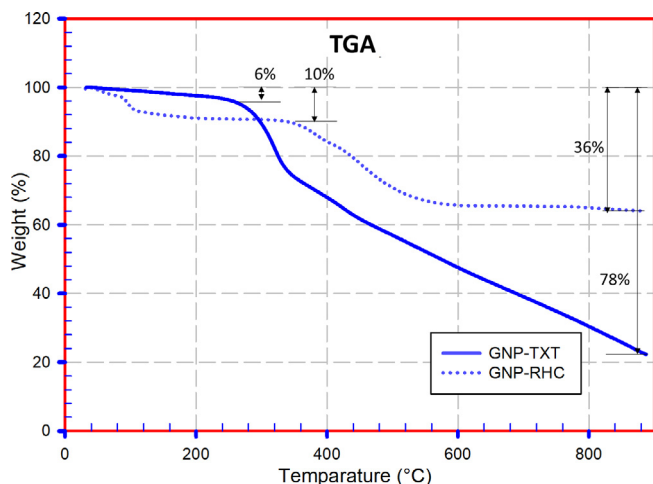


Fig. 4. TGA spectra for GNP-RHC and GNP-TXT.

ple (Ahmad et al., 2020). For the synthesized GNP-RHC, one weight loss step occurred at around 65–120 °C, while the other occurred at around 310–550 °C, the latter from the thermal decomposition of the GNP-RHC structure. When the temperature is raised to 300 °C, there is only a 10% decrease in GNP-TXT weight. Up to 885 °C for the modified GNP-TXT, there was an approximate 78% loss of weight which may be credited to the thermal degradation of the dispersants (Qamar et al., 2019). The modified GNP-TXT loses about 6% of its weight at 270 °C as opposed to 10% for the unmodified GNP-RHC at the same temperature, making it more thermally stable than the unmodified GNP-RHC.

### 3.1.4. FESEM and EDX analysis

FESEM is a technique of investigation that utilizes electron scanning. An image of a sample's surface can be acquired using this method. In addition to obtaining a high-magnification image of a sample, it also identifies the surface characteristics and composition of the sample. The FESEM can only display a sample's surface morphology (Plank and Gossen, 1991). GNP-RHC and GNP-TXT's surface composition and morphology were studied using FESEM analysis. The magnified image of the GNP-RHC, which is presented in Fig. 5a, clearly shows areas of hoary graphene sheets (see the red circle), indicating some clusters of graphene sheets are present. It appears that the GNP-RHC is very thin with some wrinkles and folds (Yang et al., 2012; Zhang et al., 2013). The FESEM image (Fig. 5b) shows that there are many gaps between sheets and matrix as the surface is clearly showing the gaps. It is apparent that none of the GNP-RHC sheets are attached to an epoxy matrix (see the blue and red arrows). A composite containing Triton-graphene (GNP-TXT), on the other hand, fractures at the fracture surface (Fig. 5c). Furthermore, the sheets adhere strongly to the epoxy matrix not only due to their well-dispersed distribution but also due to their excellent adhesion. Fig. 5d shows that the majority of Triton-graphene on the fracture surface appears to be broken (see the black arrows in that Fig. 5d). A few sheets are partially pulled away from the surface after being wrapped with an epoxy matrix (the dots on black circles indicate this). The ends of others appear to be tightly embedded in the matrix and appear to have been broken on the surface. Triton-modified GNP-RHC is compact, and most sheets lie flat on the substrate due to the relatively smooth surface (Yang et al., 2012). It was confirmed from the findings above that the non-covalent functionalization of GNP-RHC with the surfactant significantly improved dispersion and interface.

In addition, an EDX analysis was performed to confirm the formation of the nanocomposite GNP-TXT as well. According to the EDX analysis of GNP-RHC (Fig. 6a), it was discovered that there are numerous impurities present, including K, Si, Na, and Mg, which are believed to have originated from the materials used during the synthesis process (M. S. Ismail et al., 2019; Okenwa et al., 2022; Torres et al., 2021; Uda et al., 2021). The analysis of GNP-TXT (Fig. 6b) concluded that there was a considerable decrease in the amount of impurities present, demonstrating that the modification process had been successful in removing those elements from GNP-RHC. In Fig. 6(b), the EDX spectrum of the modified GNP-RHC nanocomposite is presented, which shows a higher percentage (95.1%) of C and O compared to the unmodified sample. This finding further supports the formation of GNP-TXT.

### 3.1.5. Zeta potential analysis

Prior to dispersion in WBM, GNPs must be evaluated for stability and their ability to improve drilled cutting transport efficiency. In aqueous environments, GNPs can interact with other additives because of their small size and high surface energy. A problem with NPs is their ability to agglomerate and sediment, which can result in unwanted properties in the drilling fluids and filtrates (Al-

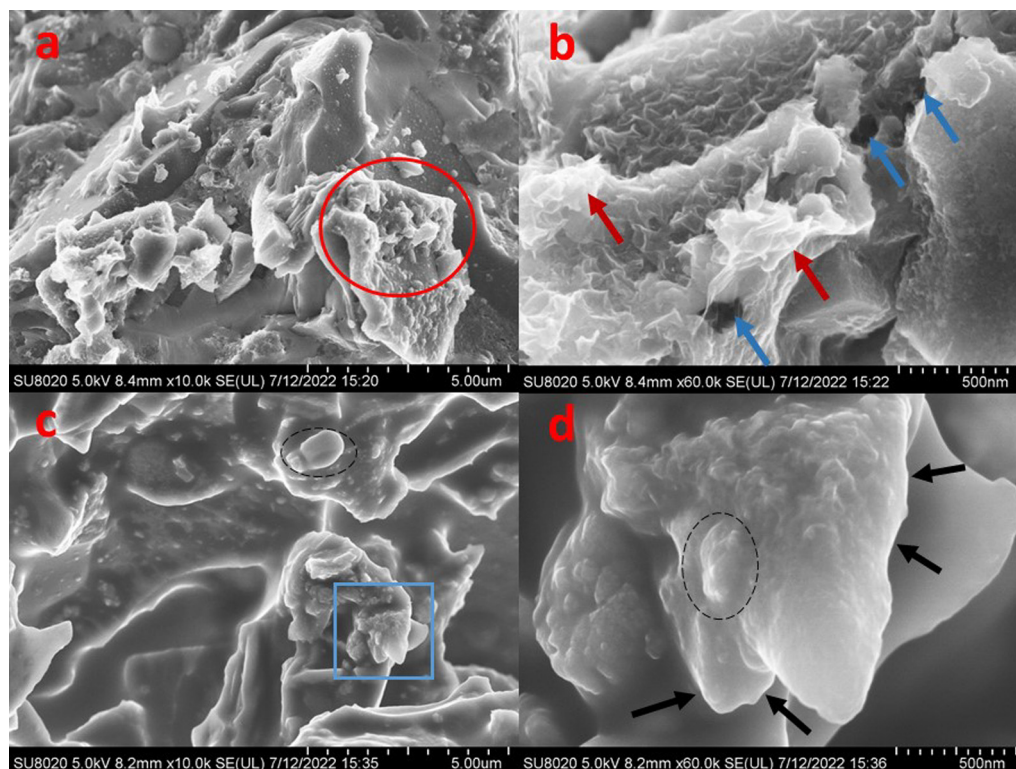


Fig. 5. FESEM images of GNP-RHC (a and b) and GNP-TXT (c and d).

Anssari et al., 2016). In colloidal dispersions, the zeta potential measures the effective surface charge of a double layer surrounding a colloidal particle and provides information regarding its stability (Konkena and Vasudevan, 2012). GNP-RHC and GNP-TXT aqueous dispersions have different zeta potentials at different pH values as shown in Fig. 7. Previously reported values (Marques et al., 2011) are consistent with these findings. As can be seen from the results, GNP-RHC sheets (Fig. 7a) have a negative charge of  $-38$  mV at pH levels 3 to 9. It's possible to form stable dispersions of GNP-RHC sheets in a pH range of 6 to 11.5 where the highest value is  $-42$  mV at pH 11.3 GNP-RHC is characterized by oxygen species at the surface, which explains this value. On the other hand, GNP-TXT (Fig. 7a) has a slightly lower zeta potential value, which indicates a lower charge density for this graphene type. At pH values between 5.8 and 11.8 zeta values of  $-35$  mV were observed, while  $-40$  mV were identified at pH levels between 10 and 11.3. GNP-RHC and GNP-TXT were determined to have zeta potentials of  $-42$  and  $-40$  mV, respectively, indicating they cannot agglomerate easily (Smith et al., 2010; White et al., 2007). The surface zeta potential results obtained are quite similar to those previously reported (Liu et al., 2018).

### 3.1.6. HRTEM analysis

The HRTEM method is the most efficient and direct method for studying layer numbers at a microscopic level. A crumpled GNP-RHC topology is displayed in Fig. 8(c). Stacks of layers appear as lighter patches, while monolayers appear as darker patches. Despite microscopic buckling, bending, and crumpling, the 2-D structure is thermally stable from its wrinkled appearance (Saleh et al., 2020). An average size of  $\sim 9$  to  $17$  nm is shown in red on Fig. 8(c) of the TEM image of the GNP-RHC sheet. Although the layers are defective, there are a few layers along the folded edge rather than a monolayer. GNP-RHC HRTEM images are depicted in Fig. 8(d) by a few layers around 8 (Kumar et al., 2016).

Here are the TEM images of modified GNP-RHC (GNP-TXT) as shown in Fig. 8(a). As can be seen in the image, the surface of GNP-RHC changed significantly after it was modified. In Fig. 8(b), the HRTEM image shows that the modified are still tightly adherent and distributed after ultrasonic pre-treatment for TEM testing. This HRTEM image clearly shows the wrinkled GNP-TXT that is transparent. Many dark lines appeared on the sheet, indicating how many layers there were. HR-TEM images of GNP-TXT show functionalized graphene layers (Hamada et al., 1992; Kataura et al., 1999). According to Fig. 8(b), many areas are still darker, indicating that some sheets are still aggregated. The surface of GNP-RHC was therefore successfully grafted with triton.

### 3.2. Mud density and pH

The mud density of all the investigated mud samples is given in Table 3 which shows that the presence of GNP-RHC and GNP-TXT gave a minor effect on the density of WBM. Density of the blank sample is 9.00 ppg. In the presence of GNP-RHC and GNP-TXT at 0.5 g, 1.0 g, 1.5 g, and 2.0 g concentrations, the density increase is less than 0.2ppg. The insignificant increase might be due to the small dimension of the additive particle size. The added NP has a negligible weight, so the mud density measurements are not affected (Ahmad et al., 2021). Base on Table 3, all the WBM samples showed that GNP-RHC and GNP-TXT had insignificant effects on mud density. 0.05 g, 1.0 g, 1.5 g, and 2.0 g concentrations of GNP-RHC and GNP-TXT increase density by approximately 0.2ppg (pounds per gallon), compared with 9.00ppg for the base mud sample. A negligible size of the additive particle could account for the insignificant increase. The density of mud is measured to reflect its ability to carry drilled cuttings in conjunction with the buoyancy effect of the suspending mud. The mud density in a drilling operation should be slightly higher than the formation pressure in order to ensure maximum penetration rate (Akpabio

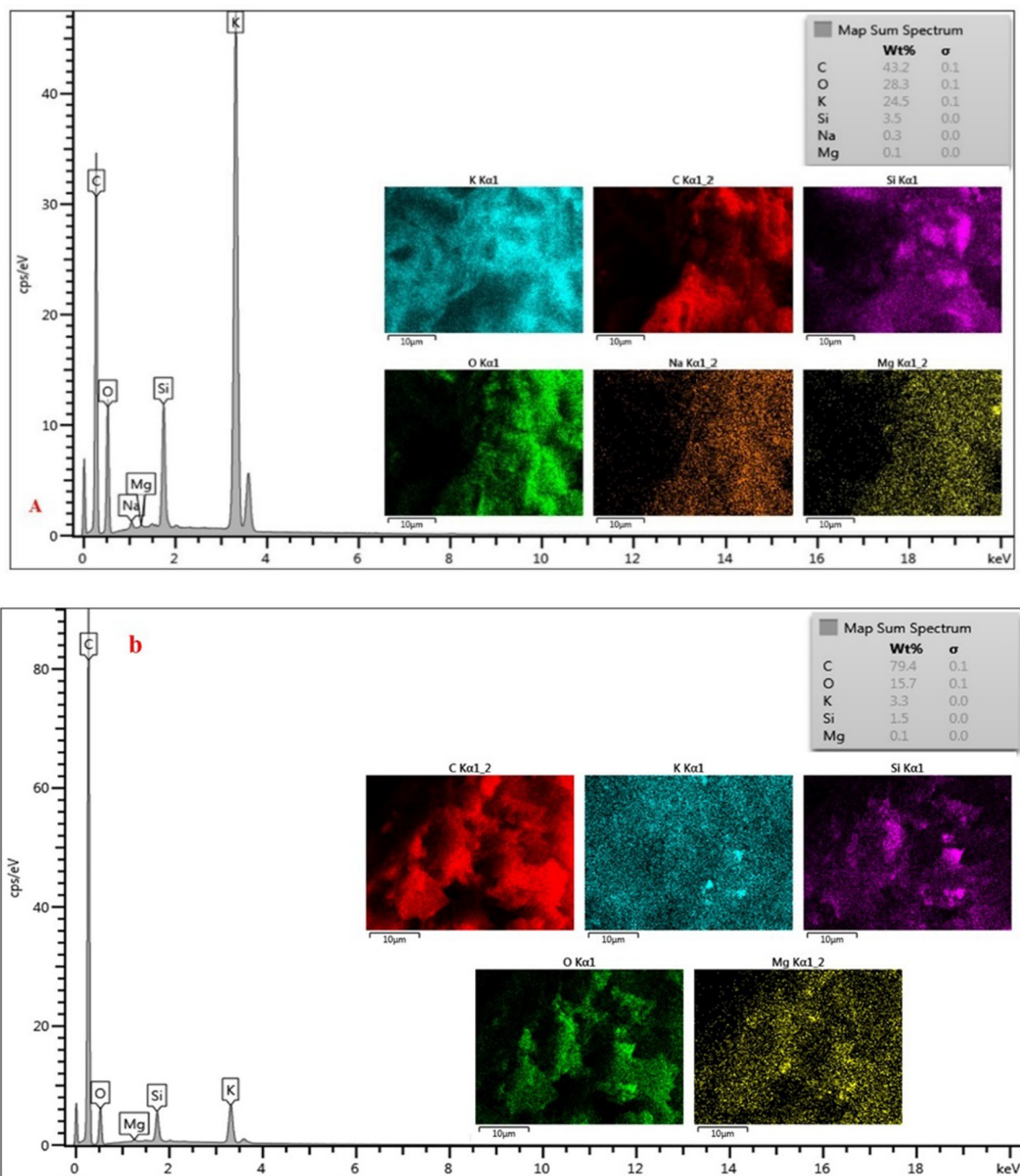


Fig. 6. EDX spectra for (a) GNP-RHC and (b) GNP-TXT.

et al., 2015). In case of excessive mud density, formation circulation will be lost, drill pipes will be stuck, penetration rate will decrease, and formation damage will occur. As a result of formation pressure higher than the hydrostatic pressure provided by the mud column, an insufficient amount of mud density (too low) will cause the well to collapse or become unstable. To ensure a successful drilling operation and remain economically viable, mud density must be chosen during the formulation stage. In the literature, similar trends of results have also been observed (Ahmad et al., 2021; Husin et al., 2018).

Adding GNP-RHC and GNP-TXT (Table 3) to the drilling fluid resulted in a minor pH decrease, which is adequate for drilling applications (Kusrini et al., 2020). Among the overall mud samples formulated, GR1 mud sample AHR caused the most significant pH decrease (7.92). Chemical additives in drilling fluid are affected by

pH levels in terms of their interaction with bentonite, their solubility, and their overall efficacy. For optimal filtration and rheological properties of WBM with bentonite, the pH should be maintained within 9–10, according to recent studies (Gamal et al., 2019; Li et al., 2018). Zeta potential analysis of the synthesized materials (Fig. 7) indicated that the materials were stable under pH (6–12) the result is also agree with figures obtained by (Gautam et al., 2018), allowing for better particle dispersion.

### 3.3. Rheological properties

It is important to consider the rheological behaviour of drilling fluid when choosing a drilling fluid. Shear thinning is the rheological phenomenon in which liquids behave in a non-Newtonian manner by having their shear viscosity decrease under shear

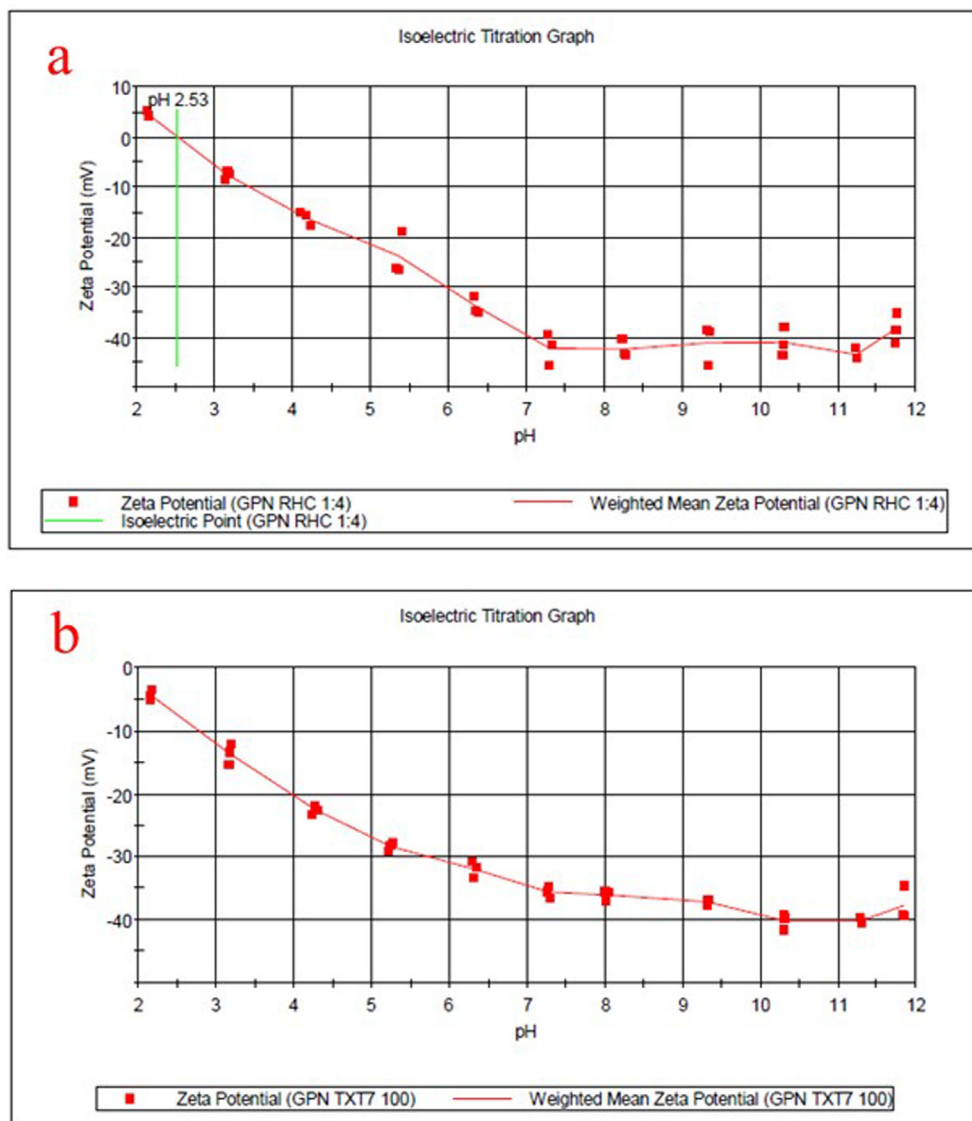


Fig. 7. Zeta potential spectra for (a) GNP-RHC (b) GNP-TXT.

(Mezger, 2006). WBM produced better rheological performance when GNP-RHC and GNP-TXT were used with varying concentrations. As shown in Table 3, the formulated drilling muds' rheological properties such as PV, YP, GS 10 sec, and GS 10 min BHR and AHR are presented.

### 3.3.1. GNP-RHC and GNP-TXT on plastic viscosity

Among other factors, plastic viscosity is determined by solid particle concentration, size, and shape, as well as the viscosity of the fluid phase. PV determines the fluid behaviour at high rates. Solid particles in the drilling fluid generate PV via mechanical friction (Ahmed et al., 2020). The effect of adding GNP-RHC and GNP-TXT nano additives (Fig. 9) was compared in varying concentrations to the base mud BHR and AHR rolling process (121 °C for 24 h). A slight decrease in PV can be seen with increasing concentration of GNP-TXT nano additive. At 1.5 g concentration, the modified nano additive recorded a viscosity value of 9 cp, which is lower than the base mud's value of 13 cp. AHR the mud formulation at 121 °C for 24 h, PV of 7cp was recorded at the same concentration. Low-PV drilling mud can drill quickly, which makes it ideal for drilling operations. Increasing GNP-TXT's repulsion of drilling fluid particles can be credited for the decrease in viscosity. In the

case of GNP-TXT, the benzene side chains are repellent to each other, resulting in high dispersion and low PV. PV is dependent on the size, shape, and concentration of solid particles in the drilling fluid phase (Committee, 2011; Ghayedi and Khosravi, 2020). An additive material with a highly negative charge can be rationalized as counteracting the positive charge of bentonite clay, which results in a lower viscosity of drilling fluid. Despite the fact that the drilling fluid's solid content will increase due to the material addition, the PV value will be lower as a result. A lower PV value provides a positive effect in drilling operations by reducing fluid circulation and lifting ability due to high-pressure drops along drill strings (Al-saba, 2018). Although the PV change in this study is infinitesimal, in a study of varying nanoadditive concentrations in WBM, a PV of (9.5–23.8 cp) was obtained, which is similar to this study's findings (Gbadamosi et al., 2018). In their study, (Paswan et al., 2016) concluded that a relatively low PV is required in order to improve cuttings lifting efficiency while drilling. Due to the presence of drilled cuttings, the viscosity of mud increases automatically. PV can be influenced by multiple factors, including temperature. As drilling goes deeper, the rise in temperature leads to a decline in PV. The data suggests that after incorporating GNP-TXT, the PV of the drilling mud significantly drops.

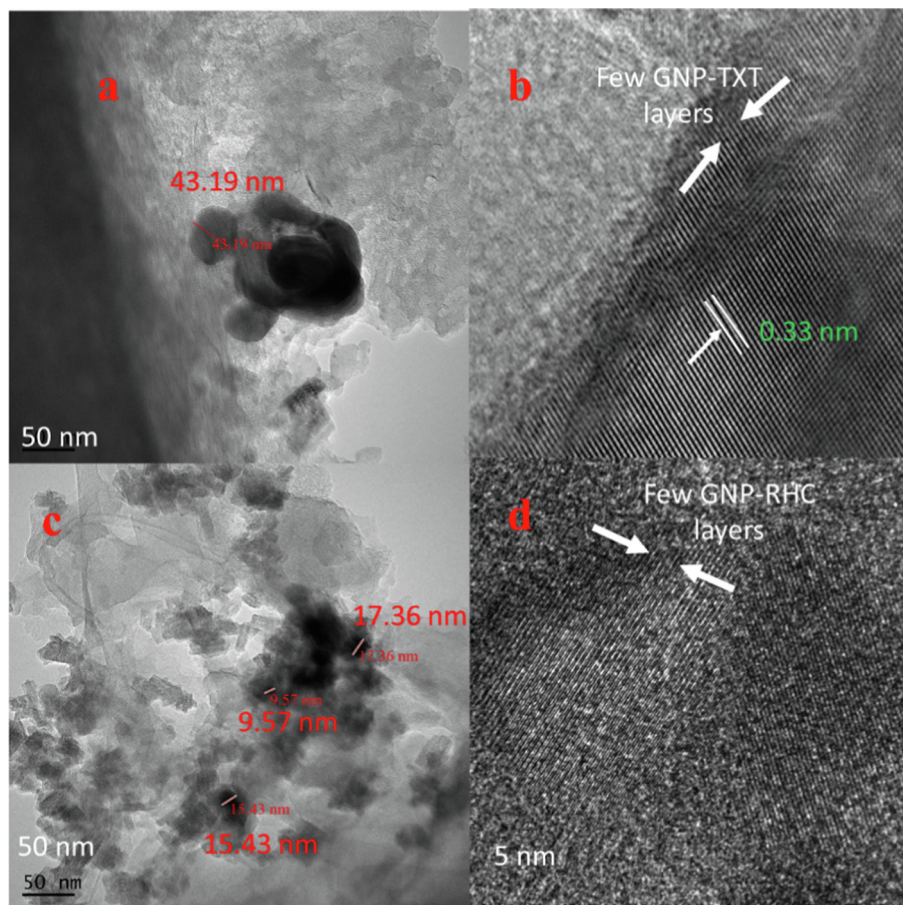


Fig. 8. TEM and HRTEM photographs of GNP-TXT: (a & b) and GNP-RHC (c & d).

Table 3

Summary of rheological properties BHR and AHR related to Figs. 9 to 11.

BHR						
Mud samples	PV (cp)	YP (lb/100ft <sup>2</sup> )	GS 10sec (lb/100ft <sup>2</sup> )	GS 10 min (lb/100ft <sup>2</sup> )	pH	Density (ppg)
Base Mud	13	63	32	40	9.5	9.0
GR1	14	66	33	41	9.25	9.0
GR2	12	66	35	43	9.34	9.1
GR3	17	61	38	45	9.41	9.1
GR4	14	66	36	46	9.48	9.2
GT1	11	80	40	42	9.12	9.1
GT2	12	80	39	41	9.2	9.1
GT3	9	79	37	38	9.28	9.15
GT4	12	65	35	37	9.31	9.2
AHR for 16 h at 120 °C						
Mud samples	PV (cp)	YP (lb/100ft <sup>2</sup> )	GS 10sec (lb/100ft <sup>2</sup> )	GS 10 min (lb/100ft <sup>2</sup> )	pH	Density (ppg)
Base Mud	8	30	54	44	8.33	8.75
GR1	9	66	45	28	7.92	8.9
GR2	9	41	22	22	7.98	9.0
GR3	7	28	16	20	8.14	9.0
GR4	8	22	10	10	8.22	9.1
GT1	8	67	40	38	8.11	9.0
GT2	7	43	34	32	8.26	9.0
GT3	7	37	28	28	8.32	9.1
GT4	6	32	21	18	8.37	9.1

### 3.3.2. Effect of GNP-RHC and GNP-TXT on yield point

The yield point (YP) is the primary resistance between the solid particles and the electrochemical gravity. It is possible to transfer cuttings from a wellbore with a high drilling fluid YP to the surface. Solid particles should be able to be transported by it if it is high enough. However, it should not exceed a certain level that puts a

lot of pressure on the pump when mud is stopped and then resumed (Bayat et al., 2018). Fig. 10 illustrates how YP responds to selected drilling fluid formulations at ambient and elevated temperatures. YP values for the base mud were determined BHR and AHR to be 63 lb/100 ft<sup>2</sup> and 30 lb/100 ft<sup>2</sup>, respectively. The YP increased by 67, 43, 37, and 32 (lb/100ft<sup>2</sup>) AHR when GNP-TXT

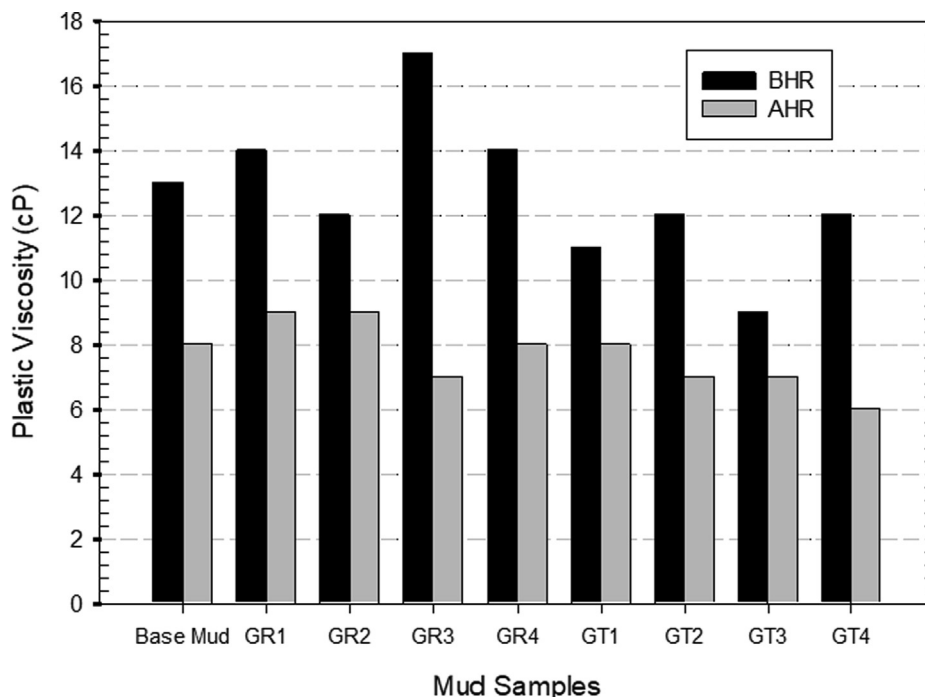


Fig. 9. GNP-RHC and GNP-TXT performance on plastic viscosity at varying concentrations BHR and AHR.

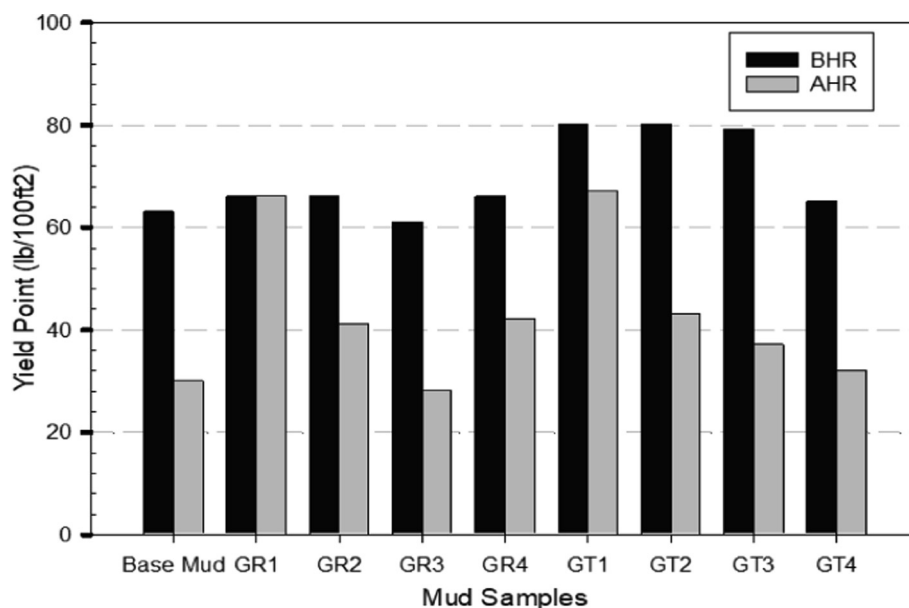


Fig. 10. GNP-RHC and GNP-TXT performance on yield point at varying concentrations BHR and AHR.

was added in varying concentrations. With respect to the formulated base mud, these increases correspond to 123%, 43%, 23%, and 6.6%. Nanoscale materials have an increased surface area, resulting in increased surface energy. This energy is reduced as a result of the particles sticking together. As a result of the nano additives in the fluid, the particles are more attracted to each other, which increases the yield point of the fluid. Increasing the yield point of a fluid has several positive effects, including improving its ability to clean drilling cuttings from wells, reducing drilling string sticking probability, and reducing the torque associated with the drill string (Hyne, 2014). It is YP that determines the ability of drilling fluid to remove drilling cuttings from beneath the drill bit

to the surface through the annulus (Ismail et al., 2016). The higher the YP, the more effective the fluid is at carrying cuttings to the surface. This is because the higher the YP, the greater the potential energy it has, which allows it to overcome the friction from the walls of the wellbore and move the cuttings efficiently. As NP concentration was increased, YP improved, which means cutting removal from boreholes to the surface will be improved (Ahmed et al., 2020). As a result of the extremely high YP values, the circulating pressure loss can increase uncontrollably, resulting in a high Equivalent Circulating Density. In Table 3, it is shown that the YP of GT1, GT2, and GT3 drilling fluid samples BHR is estimated to be slightly high. These drilling fluid samples might therefore be

unsuitable for drilling operations or for further experimentation. Nanomaterials have been used in WBM formulations before (Keshavarz Moraveji et al., 2020) with similar experimental results.

### 3.3.3. Effect of GNP-RHC and GNP-TXT on GS

As the fluid circulation in the mud stops, the GS indicates how well the fluid resists settling solid particles and cuttings. Solid particles at rest exhibit GS based on their electrochemical forces. The viscosity of a drilling mud increases with its GS, and particle settling decreases with the GS (Akpan et al., 2020). In Fig. 11(a & b), GNP-RHC and GNP-TXT are shown to influence 10 sec and 10 min GS in basic WBM. In both hot rolling and pre-rolling formulations of base mud, GS is good after 10 sec and after 10 min (Aftab et al., 2016; Jain and Mahto, 2015). As shown in Fig. 11a, the 10sec GS with the addition of GNP-RHC at elevated temperature shows a drastic decrease from 45 to 20 lb/100 ft<sup>2</sup>, which is related to a weight loss of GNP-RHC at elevated temperature as described in the TGA results (Fig. 4). It was observed that the 10sec GS for the modified GNP-RHC samples decreased slightly to a range of 40–35 lb/100 ft<sup>2</sup> BHR and to a range of 40–21 lb/100 ft<sup>2</sup> AHR. Due to the improved heat transfer features proven by the synthesized GNP-TXT materials (TGA analysis Fig. 4), the 10sec GS of the GNP-TXT samples showed lower reduction AHR than the GNP-RHC samples. It can be attributed to an appropriate distribution of nanomaterials in mud samples, which reduces the attractive forces between solid particles and increases the repulsive forces. There is no difference in the results between this study and previous research (Siti et al. 2022).

BHR, the 10 min GS (Fig. 11b) of the GNP-RHC increased as the concentration increased from 40lb/100ft<sup>2</sup> of base mud. However, AHR, the GS tends to decrease to 10lb/100ft<sup>2</sup>, corresponding to a reduction of 77.2% at 2.0 g concentration. With the application of the GNP-TXT nano additive, the 10 min GS was slightly increased by 5%, 2.5%, respectively, for 0.5 g and 1.0 g concentrations prior to hot rolling. Clay particles and graphene materials may have flocculated at the start of loading, resulting in an increase. Compared to the base mud, the 10 min GS slightly decreased at 1.5 g and 2.0 g GNP-TXT concentrations. Hot rolling, however, drastically reduced the 10 min GS value at a rate of 13.6%, 27.3%, 36.4%, and 59.1%. These values correspond to 0.5, 1.0, 1.5, and 2.0 g, respectively. When compared to the GNP-RHC, the GNP-TXT GS shows a better 'low-flat gel' trend than the GNP-RHC GS BHR and AHR. In drilling, 'low-flat gels' are preferred over 'high-flat gels', as 'high-flat gels' require higher pumping pressures to break them and resume fluid circulation. During drilling operations, this beha-

viour can result in stuck pipes (Oseh et al., 2019a; Oseh, et al., 2019b). A GNP-TXT enriched fluid formulation may be characterized by the hydrophobic non-ionic surfactant's tails self-assembling spontaneously on the surface of the organophilic clay and solid contaminants, preventing interactions between charged particles and promoting steric stabilization of the particles. Clay particles are sterically repelled by each other, resulting in lower flocculation due to electrostatic interactions (Kania et al., 2021). The results revealed that adding GNP-TXT to conventional drilling mud significantly reduced its GS after 10 s and after 10 min. As a result, the modified mud consumes less energy and is, therefore, better suited for drilling.

### 3.4. Filtration properties

#### 3.4.1. API and HPHT filtrate loss

A poor filter cake can allow deep filtrate intrusion into reservoirs, resulting in reduced oil and gas production (Saboori et al., 2018). Drilling mud has a great deal of influence on a material's ability to control FL. The filtration volume is used to analyse the plugging capability for example, less FL indicates better drilling mud performance. Compared with the base mud, the unmodified GNP-RHC and GNP-TXT exhibit lesser FL. Due to GNP-RHC and GNP-TXT films forming on the surface of filter paper, less FL can be attributed to water not flowing through the pores of filter paper. GNP-RHC and GNP-TXT API FL are shown in Fig. 12 (a & b), respectively. In response to increasing GNP-RHC concentrations, the API FL of the base mud decreased to 9.6–10.2 mL range. With an additive concentration of 1.0 g and 1.5 g of GNP-RHC, the API FL records its best result as 9.6 mL. GNP-TXT mud samples display better FL control than GNP-RHC mud samples, as shown in Fig. 12. The modified GNP-TXT sample minimized API FL by 21.8% with the 1.5 g concentration, while the base mud with GNP-RHC additive reduced it by 12.7% at the same concentration. It is likely that this behavior is the result of the fine dispersion of GNP-TXT in the drilling mud and the ability of the smaller size GNP-TXT to insert between the larger size PAC-UL and bentonite particles to plug the pore spaces between them (Mao et al., 2015).

In addition to reducing the viscosity of the liquid phase, increasing temperature also increases filtration. At a differential pressure of 500 psi and a temperature of 250 °C, Fig. 13 (a & b) show the effect of GNP-RHC and GNP-TXT on HPHT filtration properties. There was less filtrate produced by GNP-TXT additions, indicating better filtration properties. As compared to the base mud, the HPHT FL of the mud sample containing GNP-RHC decreased from

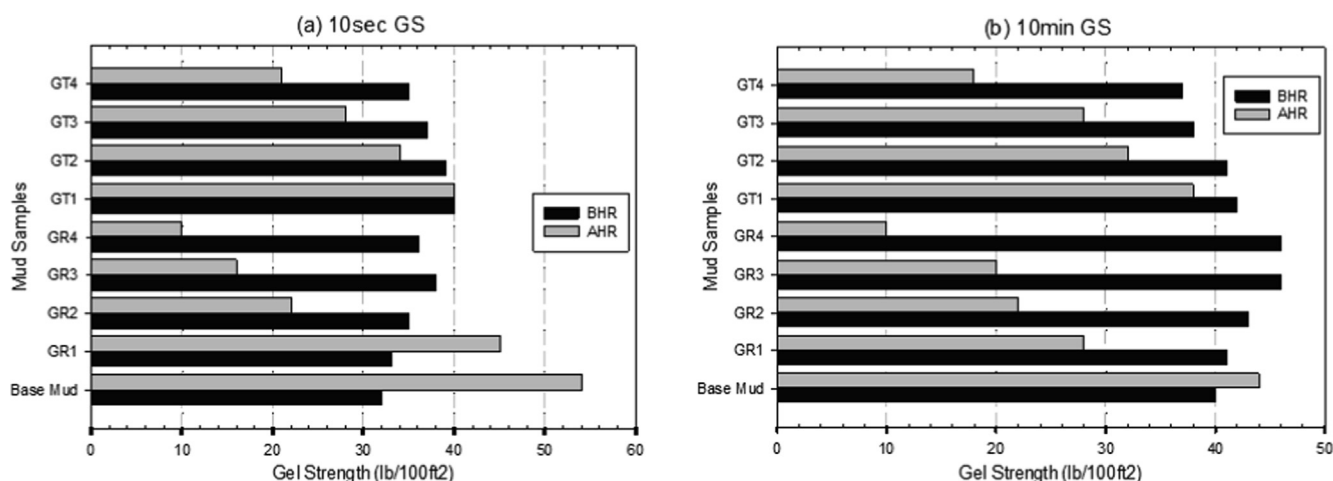


Fig. 11. GNP-RHC and GNP-TXT performance on (a) 10sec GS and (b) 10 min GS at varying concentrations BHR and AHR.

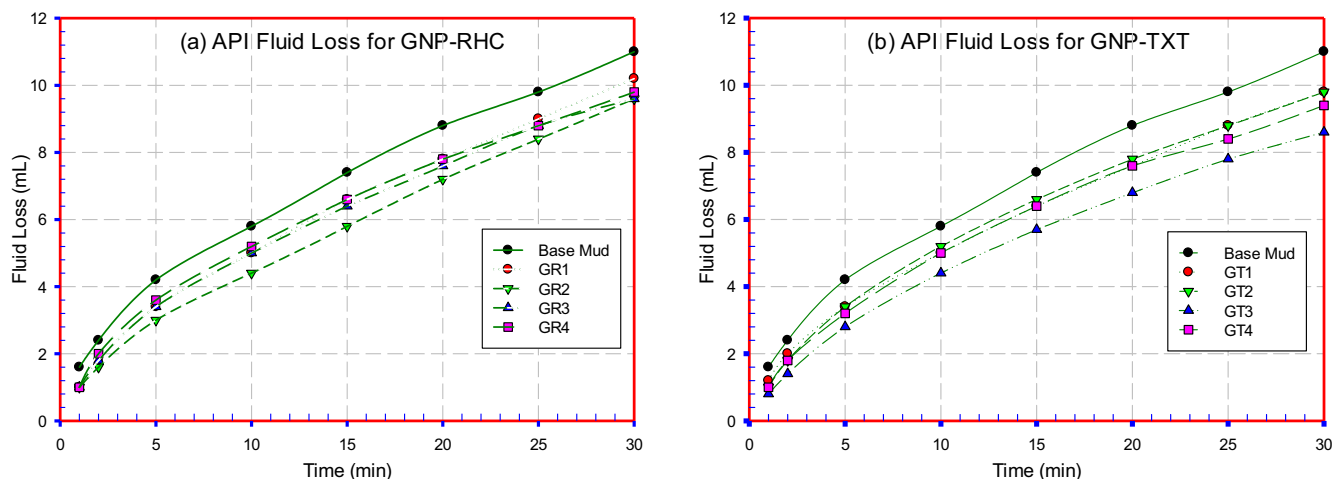


Fig. 12. API filtrate fluid loss for (a) GNP-RHC and (b) GNP-TXT performance at varying concentrations.

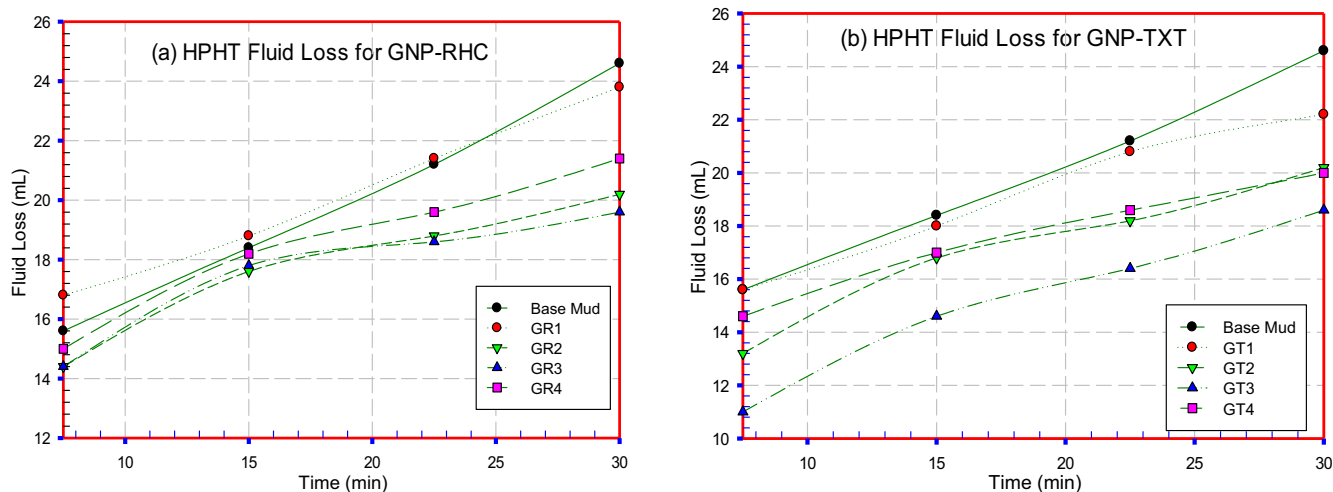


Fig. 13. HPHT filtrate fluid loss for (a) GNP-RHC and (b) GNP-TXT performance at varying concentrations.

24.6 mL to 19.6 mL at 1.5 g concentration (Fig. 13a). In comparison with GNP-RHC, the GNP-TXT mud systems performed better in terms of filtration control. This may be due to improved dispersion of the modified material additive and greater cohesion among other clay additives. A dispersant protects colloidal clay particles from aggregation into a mass of particles or flocs (Rizvi, 2009). It has been shown that dispersing solids in mud minimizes particle settlement or sagging, and this decreases fluid loss (Lahalih and Dairanieh, 1989; Shettigar et al., 2018; Skalle, 2011). Filtrate loss for GNP-TXT mud samples at 0.5 g, 1.0 g, 1.5 g, and 2.0 g concentrations was reduced compared to base mud samples by 9.75%, 17.9%, 24.4%, and 18.7%, respectively. In the presence of 1.5 g of the modified nano additive, HPHT filtrate loss was reduced to 18.6 mL. The study proves that GNP-TXT can minimize fluid loss to the formation by sealing the wellbore's permeable surface. Through GNP-TXT, tighter packing structures were formed, preventing fluid from leaking through the gaps between the micro-sized particles as shown in Fig. 14. As a result, filtrate flux was reduced (Aftab et al., 2017; A. R. Ismail et al., 2016; Oseh, et al., 2019a; Saleh et al., 2020).

Under high pressure, the nanosheets (GNP-RHC and GNP-TXT) were pressed into the pores of the formation, and some of the materials passed through while others remained to plug the pores.

This caused the nanosheets, which stayed in the pores, to accumulate and plug the pores, which prevented fluids from entering into the filter and decrease filtration volume as shown in Fig. 14. According to Darcy's law, small particles in the external filter cake reduce the cake's permeability, which in turn reduces the flow rate. Conversely, in real drilling operations where different forces act on a particle at the surface of the cake, a lower filtration rate causes less normal drag force. At low concentrations, GNPs were incorporated into filter cakes, which resulted in thick, loose, high porosity and permeability filter cakes, resulting in high fluid losses compared to drilling fluids containing higher concentrations of GNPs, which produced thin, compact, low permeability, and porosity filter cakes. Based on the results above, Fig. 14 illustrates the schematic illustration of filter cakes forming. In addition to covering fractures and holes in the larger particles, these NPs provide a seal that barricades fluid loss and reduces formation damage. In addition, it can be observed from Fig. 14 (b & c) that NPs invade more deeply inside porous micro channels due to the low permeable thin nano filter cake than what we see in the left image (Fig. 14a).

### 3.4.2. API and HPHT filter cake thickness

It has been noted that nano-enhanced clay drilling fluids form reasonably thin filter cakes on borehole walls, which is often con-

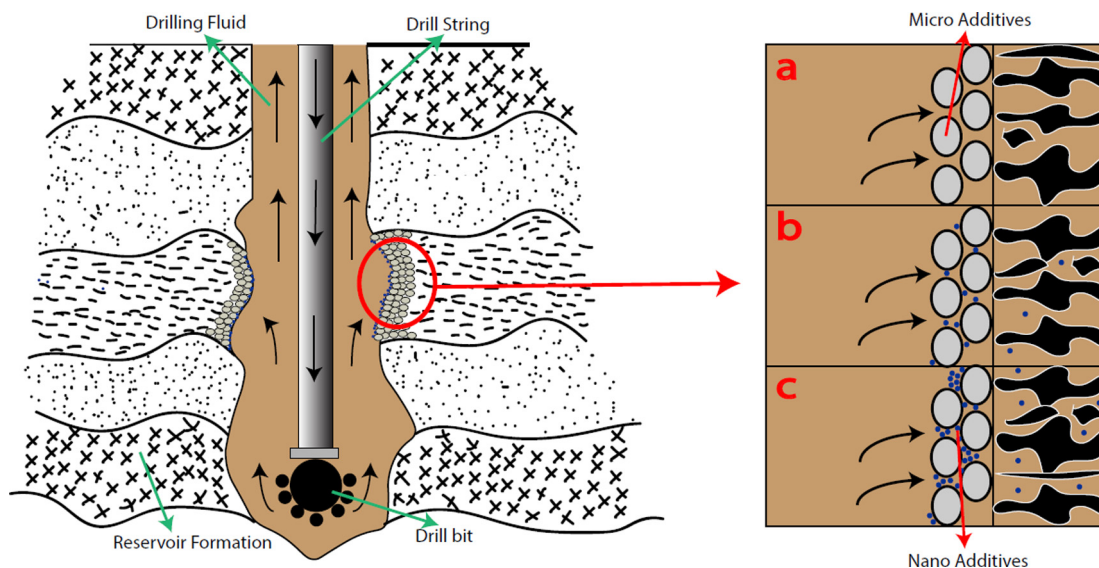


Fig. 14. Schematic illustration of Filtrate fluid loss and filter cakes formation.

Table 4

API and HPHT filter cake for GNP-RHC and GNP-TXT drilling fluid samples.

Mud Sample	Base Mud	GR1	GR2	GR3	GR4	GT1	GT2	GT3	GT4
API FCT	2.42	2.4	2.27	2.17	2.2	2.23	1.88	1.67	1.67
HPHT FCT	4.88	4.54	4.3	4.3	3.73	4.46	4.25	3.5	3.55

Table 5

Lubricity coefficient for GNP-RHC and GNP-TXT BHR and AHR at 121 °C for 16 h.

Mud Sample	Base Mud	GR1	GR2	GR3	GR4	GT1	GT2	GT3	GT4
CoF 25 °C	0.45	0.47	0.43	0.32	0.33	0.26	0.24	0.20	0.24
CoF 121 °C	0.52	0.49	0.46	0.40	0.40	0.32	0.28	0.23	0.25

sidered an improvement (Kadaster et al., 1992). Poor quality of the filter cake may lead to decreased hydrocarbon production if the deep filtrate invades the reservoir (Saboori et al., 2018). GNP-RHC and GNP-TXT API and HPHT FCT are shown in Table 4. API FCT measurements of the base mud increased to 4.88 mm at 250°C, 500psi under HPHT conditions. When 1.5 g of GNP-RHC was added to the base mud, the API FCT was reduced by 10.33%. It was observed that the GNP-TXT sample achieved a reduction of 30.99% in API FCT from the base mud at the same concentration. As compared to the samples of GNP-RHC mud, GNP-TXT mud had a lower API FCT. As described previously, the GNP-TXT particles form a seal that minimizes mud seepage through the retention by passing through the particles (Fig. 14). As a result of this behaviour, they produce lower filtrate fluxes, which results in lower cake thicknesses (Mao et al., 2015). Under HPHT conditions, all mud samples showed a decrease in FCT as concentration increased. Compared to GNP-RHC drilling muds at 250 °C and 500psi, HPHT FCT of GNP-TXT drilling muds shows a lower decreasing trajectory. These results prescribed that GNP-RHC mud samples have a higher filter cake permeability and slightly lower thermal stability at the tested temperatures (see TGA analysis results Fig. 4).

### 3.5. Lubricity measurement

Drilling in a directional or extended-reach environment is most limited by torque and drag. The lubricity coefficient plays an

important role in torque and drag (Maidla and Wojtanowicz, 1990; Quigley, 1989; Sheppard et al., 1987). Drilling operations therefore face the challenge of controlling friction. At different temperatures (25 °C and 121 °C), the coefficient of friction (CoF) of basic and nano-enriched WBM are examined. At varying temperatures, Table 5 shows how GNPs affect mud lubricity. Mud lubricity coefficient is improved by adding GNP-TXT NPs to WBM. GNPs decrease the lubricity coefficient as their concentration increases, which indicates a reduction in mud friction. At ambient and elevated temperatures, 1.5 g of GNP-TXT mud improves the lubricity coefficient most significantly to 0.2 and 0.23, respectively. A number of factors may contribute to GNP-TXT's performance. First, the GNPs formed bearings between the two metal-to-metal contacts following their sheet-like structure (Aftab et al., 2020). Moreover, triton-X100 surfactants might have coated the contact surfaces, enhancing lubricity (Amrita and Srikant, 2021; Liang et al., 2016). Base mud lubricity coefficients rise by 13.5% at 121 °C, and nano-mud coefficients rise by 14.3% at 1.0 g. As the temperature increases, PAC degradation increases, resulting in a wider space between additive molecules (Aliheidari et al., 2017; Koltzenburg et al., 2017). A result of this could be that the lubricious layer between the contact surfaces becomes unstable, increasing the CoF. Due to the improved thermal stability of the modified GNP, surfactant degradation in GNP-TXT form mud is lower than that of the base mud. The study concluded mud lubricity had improved due to a low CoF, which implies less friction.

#### 4. Summary and conclusions

This research developed an environmentally friendly nano material additive with enhanced properties through surface modification for drilling fluid application. Effects of incorporating GNP-RHC and GNP-TXT NPs prepared through synthesis and modification methods giving diverse sizes distributions and thermal stability, is investigated by measuring variations in the rheological properties, filtration loss, and lubricity of the formulated mud systems. These properties are also studied with and without NPs at different concentrations, BHR and AHR. It is concluded that:

- The chemical structure, morphology and stability of GNP-RHC and GNP-TXT nano additives were characterized by FT-IR, EDX, FESEM, TGA and Zeta Potential. FTIR and EDX confirm the functional groups on the GNP-RHC and GNP-TXT basal plane and the elemental compositions of the synthesized material. The material dispersion stability was confirmed through zeta potential analysis and studies show that both the nanomaterials are within the acceptable stability range. These analyses confirmed that all synthesized additives exhibited the desired structures.
- The rheological properties BHR and AHR of the WBM modified by synthesized additives were examined. The parameters of rheological properties such as: PV, YP, and GS improved compared to the base mud. With addition of GNP-RHC and GNP-TXT from 0.5 to 2.0 g the significant improvement occurred at rheological properties of the nano-enriched WBM. At NP concentration 1.5 g, it was observed that all the nano additives slightly decreased the PV with respect to the base mud BHR. The results revealed that adding GNP-TXT to the base mud significantly reduced its 10 s and 10 min GS AHR. It was also observed that best rheological improvement is observed with the addition of 1.0 g GT2 of the modified nano additive (GNP-TXT) into the base mud.
- The API and HPHT filtrate fluid loss and filter cake thickness of both the nano additives at varying concentrations were examined. But the best results of filtration properties were observed at base mud that were treated with 1.5 g GNP-TXT as an additive, that the API and HPHT fluid loss decreased up to 21.8% and 24.4%, respectively. The presence of GNP-RHC and GNP-TXT in water base mud significantly decreased the filter cake thickness with increasing concentration in both API and HPHT conditions.
- GNPs sheet-like morphology decreased the surface roughness between metal to metal assemblies, enhancing the lubricity of the based mud with the addition of the synthesized materials. Moreover, the surfactant present in GNP-TXT additive serves as a coating agent on the casing block and the tester's metal surface, thus providing lubricity.

From the above study, it can be concluded that the modified locally derived GNPs can be used in WBM to enhance its rheological properties and improve its filtration and lubricity characteristics. The improved dispersion ability coupled with thermal stability of the modified nano additive contributes in enhancing the basic drilling mud at elevated temperatures.

#### CRedit authorship contribution statement

**Muftahu N. Yahya:** Conceptualization. **M.N.A.M Norddin:** Writing – review & editing. **Issham Ismail:** Writing – review & editing. **A.A.A. Rasol:** Funding acquisition. **Abdul R. Risal:** Funding acquisition. **Jeffrey O.Oseh:** Writing – review & editing. **Faruk Yakasai:** Conceptualization. **Eugene N. Ngouangna:** . **Sajid Khan:** . **Muhanad Al-Ani:** .

#### Declaration of Competing Interest

The authors declare that they have no known competing financial interests or personal relationships that could have appeared to influence the work reported in this paper.

#### Acknowledgement

The authors will like to acknowledge the financial support from the Ministry of Education Malaysia under Fundamental Research Grant Scheme (FRGS) (FRGS/1/2021/TKO/UTM/02/73) and Universiti Teknologi Malaysia for the funding under UTM Fundamental Research (UTMFR) (QJ130000.3046.04M20).

#### References

- Aftab, A., Ismail, A.R., Khokhar, S., Ibutoto, Z.H., 2016. Novel zinc oxide nanoparticles deposited acrylamide composite used for enhancing the performance of water-based drilling fluids at elevated temperature conditions. *J. Pet. Sci. Eng.* 146, 1142–1157.
- Aftab, A., Ismail, A.R., Ibutoto, Z.H., 2017. Enhancing the rheological properties and shale inhibition behavior of water-based mud using nanosilica, multi-walled carbon nanotube, and graphene nanoplatelet. *Egypt. J. Pet.* 26 (2), 291–299. <https://doi.org/10.1016/j.ejpe.2016.05.004>.
- Aftab, A., Ali, M., Arif, M., Panhwar, S., Saady, N.M.C., Al-Khdheawi, E.A., Mahmoud, O., Ismail, A.R., Keshavarz, A., Iglauer, S., 2020. Influence of tailor-made TiO<sub>2</sub>/API bentonite nanocomposite on drilling mud performance: Towards enhanced drilling operations. *Appl. Clay Sci.* 199, 105862.
- Ahmad, Ali, I., Bins Safri, M. S., Bin Mohammad Faiz, M. A. I., & Zamir, A. (2021). Synergetic effects of graphene nanoplatelets/tapioca starch on water-based drilling muds: Enhancements in rheological and filtration characteristics. *Polymers*, 13(16), 2655.
- Ahmad, N., Nordin, N.A.H.M., Jaafar, J., Malek, N.A.N.N., Ismail, A.F., Yahya, M.N.F., Hanim, S.A.M., Abdullah, M.S., 2020. Eco-friendly method for synthesis of zeolitic imidazolate framework 8 decorated graphene oxide for antibacterial activity enhancement. *Particuology* 49, 24–32.
- Ahmed, N., Alam, M.S., Salam, M.A., 2020. Experimental analysis of drilling fluid prepared by mixing iron (III) oxide nanoparticles with a KCl-Glycol-PHPA polymer-based mud used in drilling operation. *J. Pet. Explor. Prod. Technol.* 10, 3389–3397.
- Akpabio, J.U., Inyang, P.N., Iheaka, C.I., 2015. The effect of drilling mud density on penetration rate. *Int. Res. J. Eng. Technol. (IRJET)* 2 (09).
- Akpan, E.U., Enyi, G.C., Nasr, G.G., 2020. Enhancing the performance of xanthan gum in water-based mud systems using an environmentally friendly biopolymer. *J. Pet. Explor. Prod. Technol.* 10, 1933–1948.
- Al-Anssari, S., Barifcani, A., Wang, S., Maxim, L., Iglauer, S., 2016. Wettability alteration of oil-wet carbonate by silica nanofluid. *J. Colloid Interface Sci.* 461, 435–442.
- Aliheidari, N., Tripuraneni, R., Ameli, A., Nadimpalli, S., 2017. Fracture resistance measurement of fused deposition modeling 3D printed polymers. *Polym. Test.* 60, 94–101. <https://doi.org/10.1016/j.polymertesting.2017.03.016>.
- Alkhamis, M., Imqam, A., 2018. New cement formulations utilizing graphene nano platelets to improve cement properties and long-term reliability in oil wells. SPE Kingdom of Saudi Arabia Annual Technical Symposium and Exhibition.
- Amanullah, M., Al-Tahini, A.M., 2009. Nano-technology-its significance in smart fluid development for oil and gas field application. SPE Saudi Arabia Sect. Tech. Sympos.
- Amanullah, M., Yu, L., 2005. Environment friendly fluid loss additives to protect the marine environment from the detrimental effect of mud additives. *J. Pet. Sci. Eng.* 48 (3–4), 199–208.
- Amrita, M., Srikant, R.R., 2021. Quantitative analysis of dispersion, cooling and lubricating properties of graphene dispersed emulsifier oil. *J. Braz. Soc. Mech. Sci. Eng.* 43 (2), 95. <https://doi.org/10.1007/s40430-021-02820-0>.
- API, A. P. I. (2009). API Recommended Practice 13B-1. *Recommended Practice for Field Testing Water-Based Drilling Fluids*; API: Washington, DC, USA.
- Arain, A.H., Ridha, S., Ilyas, S.U., Mohyaldinn, M.E., Suppiah, R.R., 2022. Evaluating the influence of graphene nanoplatelets on the performance of invert emulsion drilling fluid in high-temperature wells. *J. Pet. Explor. Prod. Technol.*, 1–25.
- Aramendiz, J., Imqam, A., 2019. Water-based drilling fluid formulation using silica and graphene nanoparticles for unconventional shale applications. *J. Pet. Sci. Eng.* 179, 742–749. <https://doi.org/10.1016/j.petrol.2019.04.085>.
- Arifin, N.F.T., Yusof, N., Nordin, N.A.H.M., Bilad, M.R., Jaafar, J., Ismail, A.F., Aziz, F., Salleh, W.N.W., 2021. Comparison of different activated agents on biomass-derived graphene towards the hybrid nanocomposites with zeolitic imidazolate framework-8 for room temperature hydrogen storage. *J. Environ. Chem. Eng.* 9 (2), 105118. <https://doi.org/10.1016/j.jece.2021.105118>.
- Bayat, A.E., Moghanloo, P.J., Piroozian, A., Rafati, R., 2018. Experimental investigation of rheological and filtration properties of water-based drilling fluids in presence of various nanoparticles. *Colloids Surf. A Physicochem. Eng. Asp.* 555, 256–263.

- Bayat, A.E., Harati, S., Kolivandi, H., 2021. Evaluation of rheological and filtration properties of a polymeric water-based drilling mud in presence of nano additives at various temperatures. *Colloids Surf. A Physicochem. Eng. Asp.* 627, 127128.
- Cameron, C. (2001). *Drilling fluids design and management for extended reach drilling. SPE/IADC Middle East Drilling Technology Conference.*
- Che Othman, F.E., Ismail, M.S., Yusof, N., Samitsu, S., Yusop, M.Z., Tajul Arifin, N.F., Alias, N.H., Jaafar, J., Aziz, F., Wan Salleh, W.N., 2020. Methane adsorption by porous graphene derived from rice husk ashes under various stabilization temperatures. *Carbon Lett.* 30, 535–543.
- Committee, A. S. S. (2011). *Drilling fluids processing handbook.* Elsevier.
- Dong, L., Joseph, K.L., Witkowski, C.M., Craig, M.M., 2008. Cytotoxicity of single-walled carbon nanotubes suspended in various surfactants. *Nanotechnology* 19 (25), 255702.
- Elkatatny, S., Tariq, Z., Mahmoud, M., 2016. Real time prediction of drilling fluid rheological properties using Artificial Neural Networks visible mathematical model (white box). *J. Pet. Sci. Eng.* 146, 1202–1210.
- Fink, J., 2015. *Water-based chemicals and technology for drilling, completion, and workover fluids.* Gulf Professional Publishing.
- Fu, P., Hu, S., Xiang, J., Li, P., Huang, D., Jiang, L., Zhang, A., Zhang, J., 2010. FTIR study of pyrolysis products evolving from typical agricultural residues. *J. Anal. Appl. Pyrol.* 88 (2), 117–123.
- Gamal, H., Elkatatny, S., Basfar, S., Al-Majed, A., 2019. Effect of pH on rheological and filtration properties of water-based drilling fluid based on bentonite. *Sustainability* 11 (23), 6714.
- Gautam, S., Guria, C., Rajak, D.K., Pathak, A.K., 2018. Functionalization of fly ash for the substitution of bentonite in drilling fluid. *J. Pet. Sci. Eng.* 166, 63–72.
- Gautam, S., Guria, C., Gope, L., 2021. Prediction of high-pressure/high-temperature rheological properties of drilling fluids from the viscosity data measured on a coaxial cylinder viscometer. *SPE J.* 26 (05), 2527–2548.
- Gbadamosi, A. O., Junin, R., Oseh, J. O., Agi, A., Yekeen, N., Abdalla, Y., Ogiriki, S. O., & Yusuff, A. S. (2018, August 6). *Improving Hole Cleaning Efficiency using Nanosilica in Water-Based Drilling Mud.* SPE Nigeria Annual International Conference and Exhibition. <https://doi.org/10.2118/193401-MS>.
- Ghayedi, A., Khosravi, A., 2020. Laboratory investigation of the effect of GO-ZnO nanocomposite on drilling fluid properties and its potential on H<sub>2</sub>S removal in oil reservoirs. *J. Pet. Sci. Eng.* 184, 106684.
- Gontarek-Castro, E., Rybarczyk, M.K., Castro-Muñoz, R., Morales-Jiménez, M., Barragán-Huerta, B., Lieder, M., 2021. Characterization of PVDF/graphene nanocomposite membranes for water desalination with enhanced antifungal activity. *Water* 13 (9), 1279.
- Guardia, L., Fernández-Merino, M.J., Paredes, J.I., Solís-Fernández, P., Villar-Rodil, S., Martínez-Alonso, A., Tascón, J.M.D., 2011. High-throughput production of pristine graphene in an aqueous dispersion assisted by non-ionic surfactants. *Carbon* 49 (5), 1653–1662.
- Hamad, B.A., He, M., Xu, M., Liu, W., Mpelwa, M., Tang, S., Jin, L., Song, J., 2020. A novel amphoteric polymer as a rheology enhancer and fluid-loss control agent for water-based drilling muds at elevated temperatures. *ACS Omega* 5 (15), 8483–8495.
- Hamada, N., Sawada, S., Oshiyama, A., 1992. New one-dimensional conductors: Graphitic microtubules. *Phys. Rev. Lett.* 68 (10), 1579.
- Hamdi, S.S., Al-Kayiem, H.H., Alsabah, M.S., Muhsan, A.S., 2022. A comparative study of dispersed and grafted nanofluids of graphene nanoplatelets with natural polymer in high salinity brine for enhanced oil recovery. *J. Pet. Sci. Eng.* 210, 110004.
- Hasan, M.L., Abidin, N.A.Z., Singh, A., 2018. The rheological performance of guar gum and castor oil as additives in water-based drilling fluid. *Mater. Today: Proc.* 5 (10), 21810–21817.
- Heshamudin, N.S., Katende, A., Rashid, H.A., Ismail, I., Sagala, F., Samsuri, A., 2019. Experimental investigation of the effect of drill pipe rotation on improving hole cleaning using water-based mud enriched with polypropylene beads in vertical and horizontal wellbores. *J. Pet. Sci. Eng.* 179, 1173–1185. <https://doi.org/10.1016/j.petrol.2019.04.086>.
- Hong, J., Kim, D., 2012. Effects of aggregation on the thermal conductivity of alumina/water nanofluids. *Thermochim. Acta* 542, 28–32.
- Hu, H., Wang, X., Wang, J., Wan, L., Liu, F., Zheng, H., Chen, R., Xu, C., 2010. Preparation and properties of graphene nanosheets-polystyrene nanocomposites via in situ emulsion polymerization. *Chem. Phys. Lett.* 484 (4–6), 247–253.
- Husin, H., Elraies, K.A., Choi, H.J., Aman, Z., 2018. Influence of graphene nanoplatelet and silver nanoparticle on the rheological properties of water based mud. *J. Appl. Sci.* 8 (8), 1386. <https://doi.org/10.3390/app8081386>.
- Hussain, S., Kovacevic, E., Berndt, J., Santhosh, N.M., Pattyn, C., Dias, A., Strunskus, T., Ammar, M.-R., Jagodar, A., Gaillard, M., 2020. Low-temperature low-power PECVD synthesis of vertically aligned graphene. *Nanotechnology* 31 (39), 395604.
- Hyne, J.N., 2014. *Dictionary of petroleum exploration, drilling & production.* Pen Well Corporation, Tulsa.
- Ibrahim, A., Ridha, S., Amer, A., Shahari, R., Ganat, T., 2019. Influence of degree of dispersion of noncovalent functionalized graphene nanoplatelets on rheological behaviour of aqueous drilling fluids. *Int. J. Chem. Eng.* 2019, 1–11. <https://doi.org/10.1155/2019/8107168>.
- Ilyas, S.U., Ridha, S., Kareem, F.A.A., 2020. Dispersion stability and surface tension of SDS-Stabilized saline nanofluids with graphene nanoplatelets. *Colloids Surf. A Physicochem. Eng. Asp.* 592, 124584.
- Irawan, S., Kinif, I., Bayuaji, R., 2018. Maximizing drilling performance through enhanced solid control system. *Platform: J. Eng.* 1 (1), 66–82.
- Ismail, A. R., Aftab, A., Ibutopo, Z. H., & zolkifile, N. (2016). *The novel approach for the enhancement of rheological properties of water-based drilling fluids by using multi-walled carbon nanotube, nanosilica and glass beads* | Elsevier Enhanced Reader. <https://doi.org/10.1016/j.petrol.2016.01.036>.
- Ismail, M.S., Yusof, N., Mohd Yusop, M.Z., Ismail, A.F., Jaafar, J., Aziz, F., Abdul Karim, Z., 2019. Synthesis and characterization of graphene derived from rice husks. *Malay. J. Fundamental Appl. Sci.* 15 (4), 516–521. <https://doi.org/10.11113/mjfas.v15n4.1228>.
- Jain, R., Mahto, V., 2015. Evaluation of polyacrylamide/clay composite as a potential drilling fluid additive in inhibitive water based drilling fluid system. *J. Pet. Sci. Eng.* 133, 612–621.
- James, D.K., Tour, J.M., 2013. Graphene: Powder, flakes, ribbons, and sheets. *Acc. Chem. Res.* 46 (10), 2307–2318.
- Jiang, L., Li, C., Wang, C., Xu, N., Chu, H., 2018. Utilization of flue gas desulfurization gypsum as an activation agent for high-volume slag concrete. *J. Clean. Prod.* 205, 589–598.
- Kania, D., Yunus, R., Omar, R., Rashid, S.A., Jan, B.M., Aulia, A., 2021. Lubricity performance of non-ionic surfactants in high-solid drilling fluids: A perspective from quantum chemical calculations and filtration properties. *J. Pet. Sci. Eng.* 207, 109162.
- Kataura, H., Kumazawa, Y., Maniwa, Y., Umez, I., Suzuki, S., Ohtsuka, Y., Achiba, Y., 1999. Optical properties of single-wall carbon nanotubes. *Synth. Met.* 103 (1–3), 2555–2558.
- Keshavarz Moraveji, M., Ghaffarkhah, A., Agin, F., Talebkeikhah, M., Jahanshahi, A., Kalantar, A., Amirhosseini, S.F., Karimifard, M., Mortazavipour, S.I., Sehat, A.A., Arjmand, M., 2020. Application of amorphous silica nanoparticles in improving the rheological properties, filtration and shale stability of glycol-based drilling fluids. *Int. Commun. Heat Mass Transfer* 115, 104625. <https://doi.org/10.1016/j.icheatmasstransfer.2020.104625>.
- Koltzenburg, S., Maskos, M., Nuyken, O., 2017. Amorphous Polymers. In: Koltzenburg, S., Maskos, M., Nuyken, O. (Eds.), *Polymer Chemistry.* Springer, pp. 119–139. [https://doi.org/10.1007/978-3-662-49279-6\\_6](https://doi.org/10.1007/978-3-662-49279-6_6).
- Konkena, B., Vasudevan, S., 2012. Understanding aqueous dispersibility of graphene oxide and reduced graphene oxide through p K a measurements. *J. Phys. Chem. Lett.* 3 (7), 867–872.
- Kosynkin, D.V., Ceriotti, G., Wilson, K.C., Lomeda, J.R., Scorsone, J.T., Patel, A.D., Friedheim, J.E., Tour, J.M., 2012. Graphene oxide as a high-performance fluid-loss-control additive in water-based drilling fluids. *ACS Appl. Mater. Interfaces* 4 (1), 222–227. <https://doi.org/10.1021/am2012799>.
- Kumar, S.B., Guo, J., 2011. Multilayer graphene under vertical electric field. *Appl. Phys. Lett.* 98 (22), 222101.
- Kumar, R., Singh, R.K., Singh, D.P., 2016. Natural and waste hydrocarbon precursors for the synthesis of carbon based nanomaterials: Graphene and CNTs. *Renew. Sustain. Energy Rev.* 58, 976–1006. <https://doi.org/10.1016/j.rser.2015.12.120>.
- Kusrini, E., Oktavianto, F., Usman, A., Mawarni, D.P., Alhamid, M.I., 2020. Synthesis, characterization, and performance of graphene oxide and phosphorylated graphene oxide as additive in water-based drilling fluids. *Appl. Surf. Sci.* 506, 145005. <https://doi.org/10.1016/j.apsusc.2019.145005>.
- Lahalih, S.M., Dairanieh, I.S., 1989. Development of novel polymeric drilling mud dispersants. *Eur. Polym. J.* 25 (2), 187–192.
- Li, M.-C., Wu, Q., Song, K., French, A.D., Mei, C., Lei, T., 2018. PH-responsive water-based drilling fluids containing bentonite and chitin nanocrystals. *ACS Sustain. Chem. Eng.* 6 (3), 3783–3795.
- Liang, S., Shen, Z., Yi, M., Liu, L., Zhang, X., Ma, S., 2016. In-situ exfoliated graphene for high-performance water-based lubricants. *Carbon* 96, 1181–1190. <https://doi.org/10.1016/j.carbon.2015.10.077>.
- Liu, F., Yang, D., Liu, Y., Cao, Q., Sun, Y., Wang, Q., Tang, H., 2018. Improving dispersive property, biocompatibility and targeting gene transfection of graphene oxide by covalent attachment of polyamidoamine dendrimer and glycyrrhithinic acid. *Colloids Surf. B Biointerfaces* 171, 622–628.
- Maidla, E.E., Wojtanowicz, A.K., 1990. Laboratory study of borehole friction factor with a dynamic-filtration apparatus. *SPE Drill. Eng.* 5 (03), 247–255.
- Majid, N.F.F., Katende, A., Ismail, I., Sagala, F., Sharif, N.M., Yunus, M.A.C., 2019. A comprehensive investigation on the performance of durian rind as a lost circulation material in water based drilling mud. *Petroleum* 5 (3), 285–294.
- Mao, H., Qiu, Z., Shen, Z., Huang, W., 2015. Hydrophobic associated polymer based silica nanoparticles composite with core-shell structure as a filtrate reducer for drilling fluid at ultra-high temperature. *J. Pet. Sci. Eng.* 129, 1–14.
- Marques, P., Gonçalves, G., Cruz, S., Almeida, N., Singh, M., Grácio, J., Sousa, A., 2011. Functionalized graphene nanocomposites. *Adv. Nanocompos. Technol.* 11, 247–272.
- Massion, C., Lu, Y., Crandall, D., Bunker, A., Radonjic, M., 2022. Graphene nanoplatelets reinforced cement as a solution to leaky wellbores reinforcing weak points in hydrated Portland cement with graphene nanoparticles improves mechanical and chemical durability of wellbore cements. *Cem. Concr. Compos.* 133, 104726.
- Medhi, S., Chowdhury, S., Bhatt, N., Gupta, D.K., Rana, S., Sangwai, J.S., 2021. Analysis of high performing graphene oxide nanosheets based non-damaging drilling fluids through rheological measurements and CFD studies. *Powder Technol.* 377, 379–395. <https://doi.org/10.1016/j.powtec.2020.08.053>.
- Mezger, T. G. (2006). *The Rheology Handbook: For users of rotational and oscillatory rheometers.* Vincentz Network GmbH & Co. KG, Hannover, Germany.
- Morrison, I. D., & Ross, S. (2002). *Colloidal dispersions: Suspensions, emulsions, and foams.* Wiley-Interscience New York.

- Muramatsu, H., Kim, Y.A., Yang, K.-S., Cruz-Silva, R., Toda, I., Yamada, T., Terrones, M., Endo, M., Hayashi, T., Saitoh, H., 2014. Rice husk-derived graphene with nano-sized domains and clean edges. *Small* 10 (14), 2766–2770.
- Okenwa, C., Aigbodion, V.S., Offor, P.O., 2022. High performance supercapacitor active electrode material by drop-casting of graphite and graphene synthesized from rice husk. *Int. J. Adv. Manuf. Technol.* 123 (1), 657–664. <https://doi.org/10.1007/s00170-022-10166-7>.
- Oseh, J.O., Norddin, M.M., Ismail, I., Gbadamosi, A.O., Agi, A., Mohammed, H.N., 2019a. A novel approach to enhance rheological and filtration properties of water-based mud using polypropylene-silica nanocomposite. *J. Pet. Sci. Eng.* 181, 106264.
- Oseh, J.O., Norrdin, M.N.A.M., Farooqi, F., Ismail, R.A., Ismail, I., Gbadamosi, A.O., Agi, A.J., 2019b. Experimental investigation of the effect of henna leaf extracts on cuttings transportation in highly deviated and horizontal wells. *J. Pet. Explor. Prod. Technol.* 9 (3), 2387–2404. <https://doi.org/10.1007/s13202-019-0631-z>.
- Oseh, J.O., Mohd Norrdin, M.N.A., Ismail, I., Gbadamosi, A.O., Agi, A., Ismail, A.R., 2020. Study of cuttings lifting with different annular velocities using partially hydrolyzed polyacrylamide and enriched polypropylene-nanosilica composite in deviated and horizontal wells. *Appl. Nanosci.* 10 (3), 971–993. <https://doi.org/10.1007/s13204-019-01163-6>.
- Oseh, J.O., Norrdin, M.N.A.M., Ismail, I., Duru, U.I., Gbadamosi, A.O., Agi, A., Nguouangna, E.N., Bilkoor, S.O., Yahya, M.N., Risal, A.R., 2023. Rheological and filtration control performance of water-based drilling muds at different temperatures and salt contaminants using surfactant-assisted novel nanohydroxyapatite. *Geoenergy Sci. Eng.* 228, 211994. <https://doi.org/10.1016/j.geoen.2023.211994>.
- Paswan, B.K., Jain, R., Sharma, S.K., Mahto, V., Sharma, V.P., 2016. Development of Jatrophia oil-in-water emulsion drilling mud system. *J. Pet. Sci. Eng.* 144, 10–18.
- Perumalsamy, J., Gupta, P., Sangwai, J.S., 2021. Performance evaluation of esters and graphene nanoparticles as an additives on the rheological and lubrication properties of water-based drilling mud. *J. Pet. Sci. Eng.* 204, 108680.
- Pirazad, A., Shahbazi, K., & Tanha, A. A. (2018). *Enhancement of polymeric water-based drilling fluid properties using nanoparticles—ScienceDirect*. <https://www.sciencedirect.com/science/article/pii/S0920410518305709?via%3Dihub>.
- Plank, J.P., Gossen, F.A., 1991. Visualization of fluid-loss polymers in drilling-mud filter cakes. *SPE Drill. Eng.* 6 (03), 203–208.
- Qamar, S., Yasin, S., Ramzan, N., Iqbal, T., Akhtar, M.N., 2019. Preparation of stable dispersion of graphene using copolymers: Dispersivity and aromaticity analysis. *Soft Mater.* 17 (2), 190–202. <https://doi.org/10.1080/1539445X.2019.1583673>.
- Quigley, M. C. (1989). Advanced technology for laboratory measurements of drilling fluid friction coefficient. *SPE Annual Technical Conference and Exhibition*.
- Rafieefar, A., Sharif, F., Hashemi, A., Bazargan, A.M., 2021. Rheological behavior and filtration of water-based drilling fluids containing graphene oxide: Experimental measurement, mechanistic understanding, and modeling. *ACS Omega* 6 (44), 29905–29920. <https://doi.org/10.1021/acsomega.1c04398>.
- Raghavan, A., Sarkar, S., Nagappagari, L.R., Bojja, S., MuthukondaVenkatakrishnan, S., Ghosh, S., 2020. Decoration of graphene quantum dots on TiO<sub>2</sub> nanostructures: Photosensitizer and cocatalyst role for enhanced hydrogen generation. *Ind. Eng. Chem. Res.* 59 (29), 13060–13068.
- Raghavan, N., Thangavel, S., Venugopal, G., 2017. A short review on preparation of graphene from waste and bioprecursors. *Appl. Mater. Today* 7, 246–254.
- Ridha, S., Ibrahim, A., Shahari, R., Fonna, S., 2018. Graphene nanoplatelets as high-performance filtration control material in water-based drilling fluids. *IOP Conf. Ser.: Mater. Sci. Eng.* 352 (1), 012025.
- Rizvi, S. Q. (2009). 5 Dispersants. *Lubricant Additives: Chemistry and Applications*, 143.
- Ruiz-Hitzky, E., Darder, M., Fernandes, F.M., Zatile, E., Palomares, F.J., Aranda, P., 2011. Supported graphene from natural resources: Easy preparation and applications. *Wiley Online Library*.
- Saboori, R., Sabbaghi, S., Kalantari, A., Mowla, D., 2018. Improvement in filtration properties of water-based drilling fluid by nanocarboxymethyl cellulose/polystyrene core-shell nanocomposite. *J. Pet. Explor. Prod. Technol.* 8, 445–454.
- Safi, B., Zarouri, S., Chabane-Chaouache, R., Saidi, M., Benmounah, A., 2016. Physico-chemical and rheological characterization of water-based mud in the presence of polymers. *J. Pet. Explor. Prod. Technol.* 6, 185–190.
- Salahudeen, N., Mohammed, U., & Yahya, M. (2020). Mineralogical Characterization of Ririwai Biotite and its Weighting Effect on Drilling Mud Rheology. *Day 1 Tue, August 11, 2020*, D013S004R005. <https://doi.org/10.2118/203641-MS>.
- Saleem, H., Haneef, M., Abbasi, H.Y., 2018. Synthesis route of reduced graphene oxide via thermal reduction of chemically exfoliated graphene oxide. *Mater. Chem. Phys.* 204, 1–7.
- Saleh, T.A., Rana, A., Arfaj, M.K., 2020. Graphene grafted with polyethyleneimine for enhanced shale inhibition in the water-based drilling fluid. *Environ. Nanotechnol. Monit. Manage.* 14, 100348. <https://doi.org/10.1016/j.enmm.2020.100348>.
- Salih, A.H., Bilgesu, H., 2017. Investigation of rheological and filtration properties of water-based drilling fluids using various anionic nanoparticles. *SPE Western Regional Meet.*
- Salih, A.H., Elshehabi, T.A., Bilgesu, H.I., 2016. Impact of nanomaterials on the rheological and filtration properties of water-based drilling fluids. *SPE Eastern Regional Meet.*
- Sankar, S., Lee, H., Jung, H., Kim, A., Ahmed, A.T.A., Inamdar, A.I., Kim, H., Lee, S., Im, H., Kim, D.Y., 2017. Ultrathin graphene nanosheets derived from rice husks for sustainable supercapacitor electrodes. *New J. Chem.* 41 (22), 13792–13797.
- Sensoy, T., Chenevert, M. E., & Sharma, M. M. (2009). Minimizing water invasion in shale using nanoparticles. *SPE Annual Technical Conference and Exhibition*.
- Sheppard, M.C., Wick, C., Burgess, T., 1987. Designing well paths to reduce drag and torque. *SPE Drill. Eng.* 2 (04), 344–350.
- Shettigar, R.R., Misra, N.M., Patel, K., 2018. CTAB grafted PAM gel and its application in drilling fluid. *J. Pet. Sci. Eng.* 160, 129–135.
- Sie Yon, L., Gonawan, F.N., Kamaruddin, A.H., Uzir, M.H., 2013. Enzymatic deracemization of (R, S)-ibuprofen ester via lipase-catalyzed membrane reactor. *Ind. Eng. Chem. Res.* 52 (27), 9441–9453.
- Singh, P., Bahadur, J., Pal, K., 2017. One-step one chemical synthesis process of graphene from rice husk for energy storage applications. *Graphene* 6 (3), 61–71.
- Skalle, P. (2011). *Drilling Fluid Engineering*, 132.
- Smith, R.J., Lotya, M., Coleman, J.N., 2010. The importance of repulsive potential barriers for the dispersion of graphene using surfactants. *New J. Phys.* 12 (12), 125008.
- Sudhan, N., Subramani, K., Karnan, M., Ilayaraja, N., Sathish, M., 2017. Biomass-derived activated porous carbon from rice straw for a high-energy symmetric supercapacitor in aqueous and non-aqueous electrolytes. *Energy Fuel* 31 (1), 977–985.
- Sultanov, F.R., Daulbayev, C., Bakbolat, B., Mansurov, Z.A., Urazgaliyeva, A.A., Ebrahim, R., Pei, S.S., Huang, K.-P., 2020. Microwave-enhanced chemical vapor deposition graphene nanoplatelets-derived 3D porous materials for oil/water separation. *Carbon Lett.* 30, 81–92.
- Sun, X., Wu, Q., Zhang, J., Qing, Y., Wu, Y., Lee, S., 2017. Rheology, curing temperature and mechanical performance of oil well cement: Combined effect of cellulose nanofibers and graphene nano-platelets. *Mater. Des.* 114, 92–101.
- Szunerits, S., Boukherroub, R., 2016. Antibacterial activity of graphene-based materials. *J. Mater. Chem. B* 4 (43), 6892–6912.
- Tabatabaei, M., Santos, L., Al Hassan, A.A., Dahi Taleghani, A., 2022. Limiting deteriorative impacts of oil-based mud residuals on cement bonding. *SPE Annual Technical Conference and Exhibition*.
- Taha, N. M. and Lee, S. (2015, December 6). *Nano Graphene Application Improving Drilling Fluids Performance*. International Petroleum Technology Conference. <https://doi.org/10.2523/IPTC-18539-MS>.
- Tao, T., Li, G., He, Y., Yang, X., 2019. 3-D magnetic graphene balls as sorbents for cleaning oil spills. *Nanomater. Nanotechnol.* 9.
- Tchameni, A.P., Zhao, L., Ribeiro, J.X., Li, T., 2019. Predicting the rheological properties of waste vegetable oil biodiesel-modified water-based mud using artificial neural network. *Geosyst. Eng.* 22 (2), 101–111.
- Tian, X., Song, N., Yang, G., Zhou, C., Zhang, S., Zhang, P., 2022. Organic-sulfonate functionalized graphene as a high temperature lubricant for efficient antifouling and antiwear in water based drilling fluid. *Tribol. Lett.* 70 (2), 1–8.
- Tofighy, M.A., Mohammadi, T., 2019. In: Barrier, Diffusion, and Transport Properties of Rubber Nanocomposites Containing Carbon Nanofillers. Elsevier, pp. 253–285.
- Torres, F.G., Troncoso, O.P., Rodriguez, L., De-la-Torre, G.E., 2021. Sustainable synthesis, reduction and applications of graphene obtained from renewable resources. *Sustain. Mater. Technol.* 29, e00310.
- Tuck, C.O., Pérez, E., Horváth, I.T., Sheldon, R.A., Poliakoff, M., 2012. Valorization of biomass: Deriving more value from waste. *Science* 337 (6095), 695–699.
- Uda, M.N.A., Gopinath, S.C.B., Hashim, U., Halim, N.H., Parmin, N.A., Uda, M.N.A., Anbu, P., 2021. Production and characterization of graphene from carbonaceous rice straw by cost-effect extraction. *3 Biotech* 11 (5), 205. <https://doi.org/10.1007/s13205-021-02740-9>.
- Uddin, M.E., Kuila, T., Nayak, G.C., Kim, N.H., Ku, B.-C., Lee, J.H., 2013. Effects of various surfactants on the dispersion stability and electrical conductivity of surface modified graphene. *J. Alloy. Compd.* 562, 134–142.
- Valencia, C., Valencia, C.H., Zuluaga, F., Valencia, M.E., Mina, J.H., Grande-Tovar, C.D., 2018. Synthesis and application of scaffolds of chitosan-graphene oxide by the freeze-drying method for tissue regeneration. *Molecules* 23 (10), 2651.
- Wajid, A.S., Das, S., Irin, F., Ahmed, H.T., Shelburne, J.L., Parviz, D., Fullerton, R.J., Jankowski, A.F., Hedden, R.C., Green, M.J., 2012. Polymer-stabilized graphene dispersions at high concentrations in organic solvents for composite production. *Carbon* 50 (2), 526–534.
- Wang, Y., Shi, Z., Yin, J., 2011. Facile synthesis of soluble graphene via a green reduction of graphene oxide in tea solution and its biocomposites. *ACS Appl. Mater. Interfaces* 3 (4), 1127–1133.
- Wang, Z., Yu, J., Zhang, X., Li, N., Liu, B., Li, Y., Wang, Y., Wang, W., Li, Y., Zhang, L., Dissanayake, S., Suib, S.L., Sun, L., 2016. Large-scale and controllable synthesis of graphene quantum dots from rice husk biomass: A comprehensive utilization strategy. *ACS Appl. Mater. Interfaces* 8 (2), 1434–1439. <https://doi.org/10.1021/acsmi.5b10660>.
- White, B., Banerjee, S., O'Brien, S., Turro, N.J., Herman, I.P., 2007. Zeta-potential measurements of surfactant-wrapped individual single-walled carbon nanotubes. *J. Phys. Chem. C* 111 (37), 13684–13690. <https://doi.org/10.1021/jp070853e>.
- Xu, X., Guan, C., Xu, L., Tan, Y.H., Zhang, D., Wang, Y., Zhang, H., Blackwood, D.J., Wang, J., Li, M., 2019. Three dimensionally free-formable graphene foam with designed structures for energy and environmental applications. *ACS Nano* 14 (1), 937–947.
- Yang, X., Fan, K., Zhu, Y., Shen, J., Jiang, X., Zhao, P., Li, C., 2012. Tailored graphene-encapsulated mesoporous Co<sub>3</sub>O<sub>4</sub> composite microspheres for high-performance lithium ion batteries. *J. Mater. Chem.* 22 (33), 17278–17283.
- Yasin, S., Luckham, P.F., Iqbal, T., Naveed, S., 2013. Investigating the role of aromaticity of copolymers for graphitic carbon black aqueous dispersions. *Soft Mater.* 11 (4), 440–447.

- Zhang, J., Wan, S., Yan, B., Wang, L., Qian, Y., 2013. Graphene encapsulated Fe<sub>3</sub>O<sub>4</sub> nanospindles as a superior anode material for lithium-ion batteries. *J. Nanosci. Nanotechnol.* 13 (6), 4364–4369.
- Zhu, Wang, J., Holloway, B. C., Outlaw, R. A., Zhao, X., Hou, K., Shutthanandan, V., & Manos, D. M. (2007). A mechanism for carbon nanosheet formation. *Carbon*, 45 (11), 2229–2234.
- Zhu, Y., Stoller, M.D., Cai, W., Velamakanni, A., Piner, R.D., Chen, D., Ruoff, R.S., 2010. Exfoliation of graphite oxide in propylene carbonate and thermal reduction of the resulting graphene oxide platelets. *ACS Nano* 4 (2), 1227–1233.
- Zhu, Q., Wang, Y., Zhang, Y., Sun, Z., Wei, Y., Wang, R., 2018. A new generation environment friendly water-based drilling fluid and field applications. IADC/SPE Asia Pacific Drilling Technology Conference and Exhibition.